PHOTOIONIZATION BRANCHING RATIOS AND VIBRATIONAL INTENSITY DISTRIBUTIONS FOR N_2, CO, AND CO_2 BETWEEN 53 AND 75 nm

by

JAMES A. R. SAMSON AND J. L. GARDNER

Technical Report No. 1

Prepared under Grant NGR 28-004-021 by the Vacuum UV Laboratory,

University of Nebraska, Lincoln, NE 68508

For Headquarters

NATIONAL AERONAUTICS AND SPACE ADMINISTRATION

TABLE OF CONTENTS

LIST OF TABLES

LIST OF FIGURES

FIGURE PAGE

SUMMARY

This report documents the probability of radiation producing ions in specific electronic and vibrational levels. For example, when a narrow band-pass of solar ionizing photons is incident on an atmospheric species it is now possible to describe, accurately, how the radiant energy is shared among the various electronic states of the ions produced. The molecules studied were N_2, CO, and CO_2. These molecules were photoionized by radiation between 53 and 75 nm. The effects of autoionization are discussed and continuum vibrational intensities are tabulated and compared with theoretical Franck-Condon factors where available. The Branching Ratios and Partial Cross Sections for ionization into various electronic states are tabulated.

I. INTRODUCTION

The research discussed in this report is centred on the measurement of photoelectron branching ratios. When a target absorbs radiation sufficiently energetic to form an ion, the ion will in general be able to occupy a number of energy levels. By measuring the energy spectrum of the ejected electrons (i.e. photoelectron spectroscopy) the number of ions produced in each energy level may be determined. The term "branching ratio" then refers to the number of ions left in a specific energy level, as a fraction of the total number of ions formed. If the photoionization cross section is known at the same wavelength, the product of the cross section and the branching ratio gives the partial photoionization cross section at that wavelength, i.e. the cross section for ionization to a specific energy level of the ion.

The primary interest of this research was to measure photoelectron branching ratios in gases of aeronomic interest at solar wavelengths. If autoionization occurs in a gas at a given solar wavelength, it is very important that the same transition generating the line as in the sun be used in the laboratory. These emission lines generally come from highly ionized species which in general can be produced in the laboratory only in a spark type discharge which is difficult to handle experimentally. The radiation sources used in this research were DC glow discharges in helium and neon and DC arc discharges in argon and nitrogen (generated in a duoplasmatron light source).[1] The radiation was dispersed by either a ½m Seya-Namioka monochromator or a 2.2m grazing incidence monochromator. Only some of the lines used appear in the solar spectrum;[2] however, at the shorter wavelengths (less than about 65 nm) autoionization is generally absent in the molecules studied here and the branching ratios presented can be interpolated to the solar lines.

Data are presented for a number of discrete lines ranging from the first ionization thresholds in the gases N_2, CO, and CO_2 to a short wavelength limit of 52.2 nm.

If the ionization process is non-resonant (continuum ionization), the distribution over the vibrational levels of a molecule is at most a slowly changing function with the wavelength of the incident photon, and vibrational intensities have been summed to give the photoelectron branching ratio for the specific electronic states of the ion. Anomalous intensity distributions among the vibrational levels were observed at a number of wavelengths, caused by the process of autoionization. These distributions are noted at the relevant wavelengths.

II. EXPERIMENTAL TECHNIQUES

The Energy Analyzer

(1) Description

The energy analyzer used in the current study was a cylindrical mirror type with a retarding/accelerating lens. The analyzer has been described in the literature:[3] a brief summary will be given here.

The analyzer is shown schematically in Figure 1. Electrons are collected in a 6° cone centred about 54°44' to the photon beam. At this angle, the signal seen is independent of the degree of polarization of the radiation (an important feature when the radiation is dispersed because the reflection at the grating will partially polarize the radiation) and independent of the angular distribution of the ejected electrons.[4]

The electrons passing through the lens are accelerated or retarded to have a constant energy when entering the region between the two cylinders. The electrons are focused back onto the inner cylinder and then accelerated to the entrance cone of a channel electron multiplier. The multiplied current pulses are fed to the standard NIM instrumentation of a charge sensitive preamplifier and a linear amplifier, discriminated against noise pulses and then stored in a selected channel of a Nuclear Data type 2400 4096 channel store.

The voltage on the lens elements is controlled from a ramp generated either by amplifying and offsetting the analog address of the store or by a digitally programmed stepping motor driving a potentiometer, synchronized to the advance of the store. The spectrum is multiply scanned (typical dwell time of 80 ms per channel per scan) to reduce errors associated with

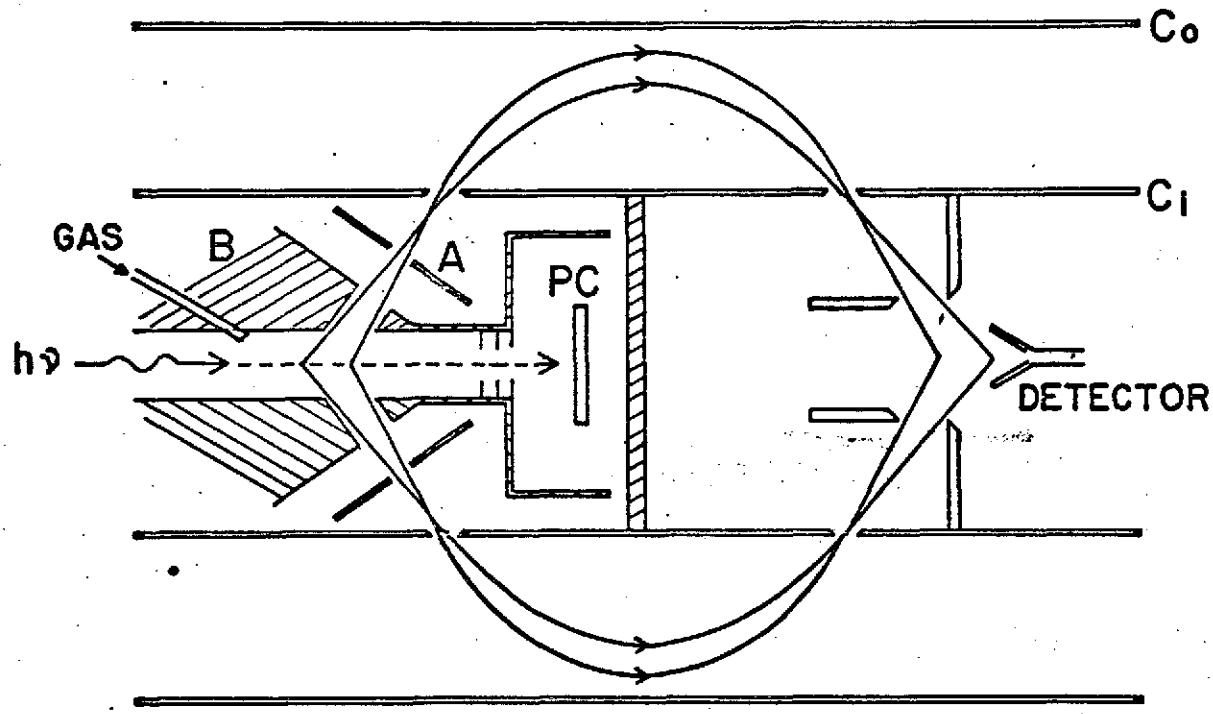

Figure 1. Schematic cross section of the cylindrical mirror electron energy analyzer.

fluctuations in the intensity of the light source or in the source gas pressure. The latter scanning method is much more accurate over long scans. Thermal drifts in the amplifiers tended to obscure the vibrational structure in spectra accumulated over a period of hours when the amplified analog address method was used.

The resolution of the analyzer, with 1 mm slits in the inner cylinder, is plotted in Figure 2 as a function of the pass energy (the kinetic energy at which the electrons must enter the region between the cylinders to pass through the exit slit to the detector). In the current analyzer, this energy (in electron volts) is 1.18 times the voltage across the two cylinders. The spectra were generally analyzed at a pass energy of 3 eV, giving a resolution of 45 meV. Figure 3 shows a spectrum recorded from H_2 at a wavelength of 73.6 nm with a pass energy of 0.75 eV; the rotational structure is clearly seen, along with the effect of increased Doppler broadening, caused by the thermal energy of the neutral molecule, as the electron energy increases.

The gas pressure in the analyzing region was typically held at 0.2 m Torr. As the pressure was increased much above this, the count rate decreased because of increased scattering out of the beam as the electrons travelled the 18 cm to the detector. The branching ratios were insensitive to pressure up to about 1 m Torr, provided the spectrum was scanned at a constant pass energy. Then for most of the path, the electrons originally formed with different energies had the same energies (the kinetic energy decreases as the electrons travel to the apex of their path, then increases again back to the same value at the inner cylinder) and suffered the same integrated scattering in the gas. If the spectrum was recorded by scanning the voltage across the two cylinders, the electrons having different kinetic energies at formation were scattered by different amounts, giving pressure sensitive

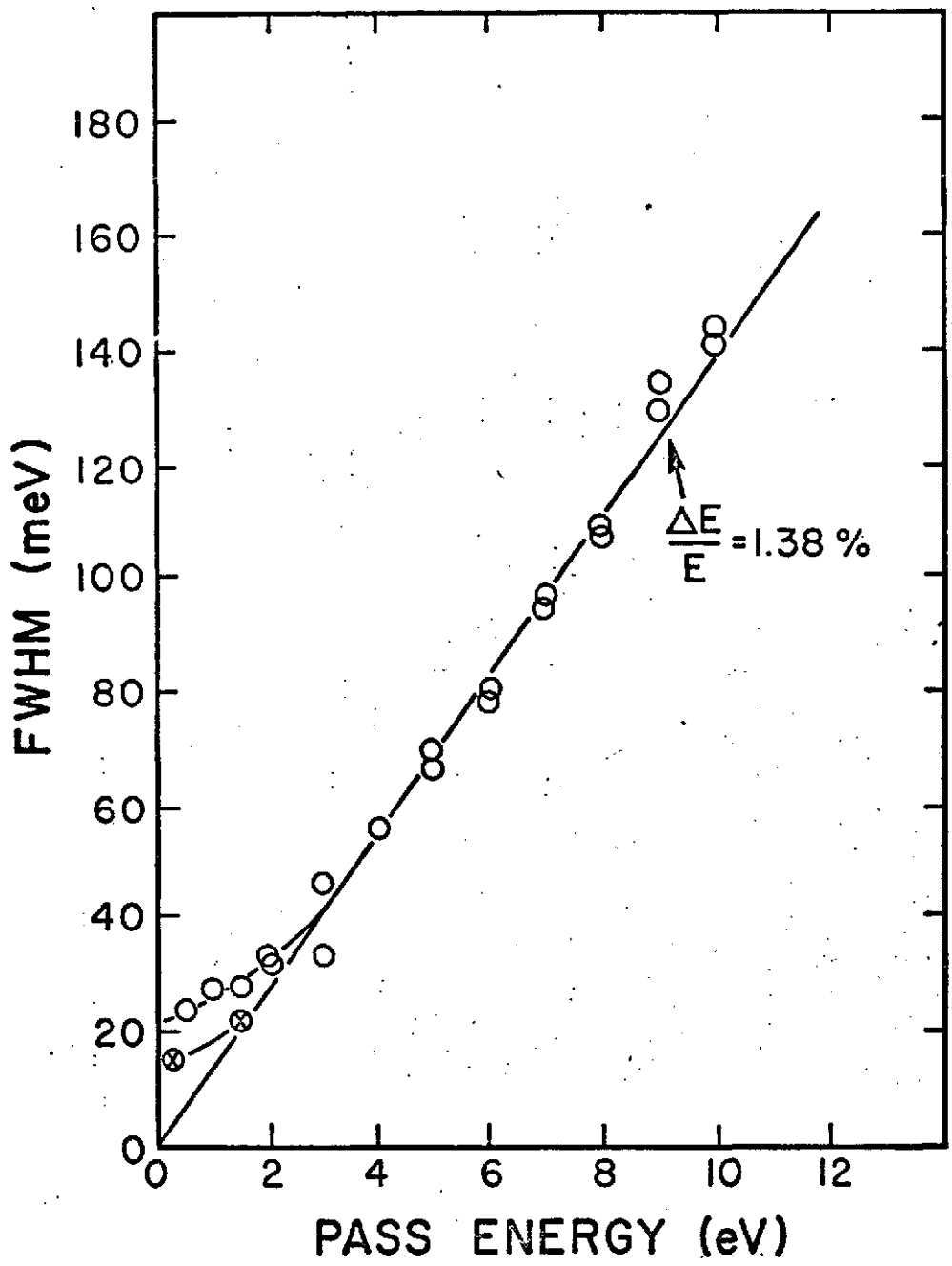

Figure 2. Resolution of the analyzer for different pass energies. o - data for xenon photoelectrons at 58.4 nm. ⊠ - data for carbon monoxide photoelectrons at 73.6 nm.

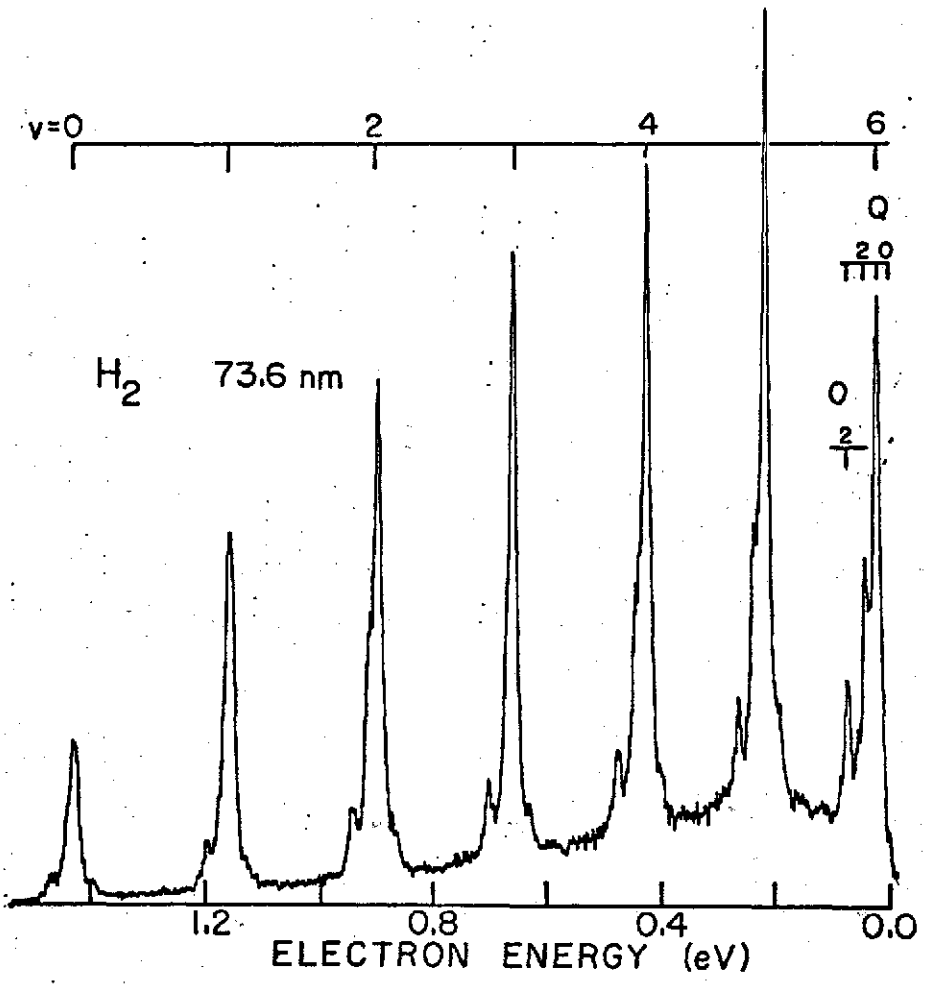

Figure 3. High resolution photoelectron spectrum recorded from hydrogen at a wavelength of 73.6 nm.

branching ratios. This is illustrated in Figure 4 for the case of CO ionized by 58.4 nm photons. The resonance in the electron scattering cross section[5] shown in the Figure is caused by the formation of CO^-; the electron energies following ionization at 58.4 nm are indicated on the scattering cross section curve. The count rate of electrons from transitions to the v=0 level of the $X\ ^2\Sigma^+$ ionic ground state, and the ratio of the measured intensities of the $A\ ^2\Pi$ and $B\ ^2\Sigma^+$ ionic electronic states, as a function of pressure, are shown for both methods of scanning. The relative intensities derived from spectra recorded at a constant pass energy are seen to be much less sensitive to the pressure than those derived from spectra recorded by scanning the voltage across the cylinders. (The ratios presented in the graphs have not been corrected for the transmission of the analyzer and should not be compared with results presented later in this report.)

Scattering effects within the ion chamber may alter the spectrum. This has been discussed in the literature.[3] The ion chamber of the analyzer used to record the branching ratios presented here was modified to provide better trapping of the unwanted electrons than previous designs, and these effects were not significant in the determination of the branching ratios.

(2) Calibration of the Collecting Efficiency

Accurate branching ratios can be obtained only if the collecting efficiency or transmission of the analyzer is known as a function of the electron energy.

The collecting efficiency of the photoelectron spectrometer described above was calibrated by recording argon and xenon photoelectron spectra at a number of different argon emission lines produced in a duoplasmatron light

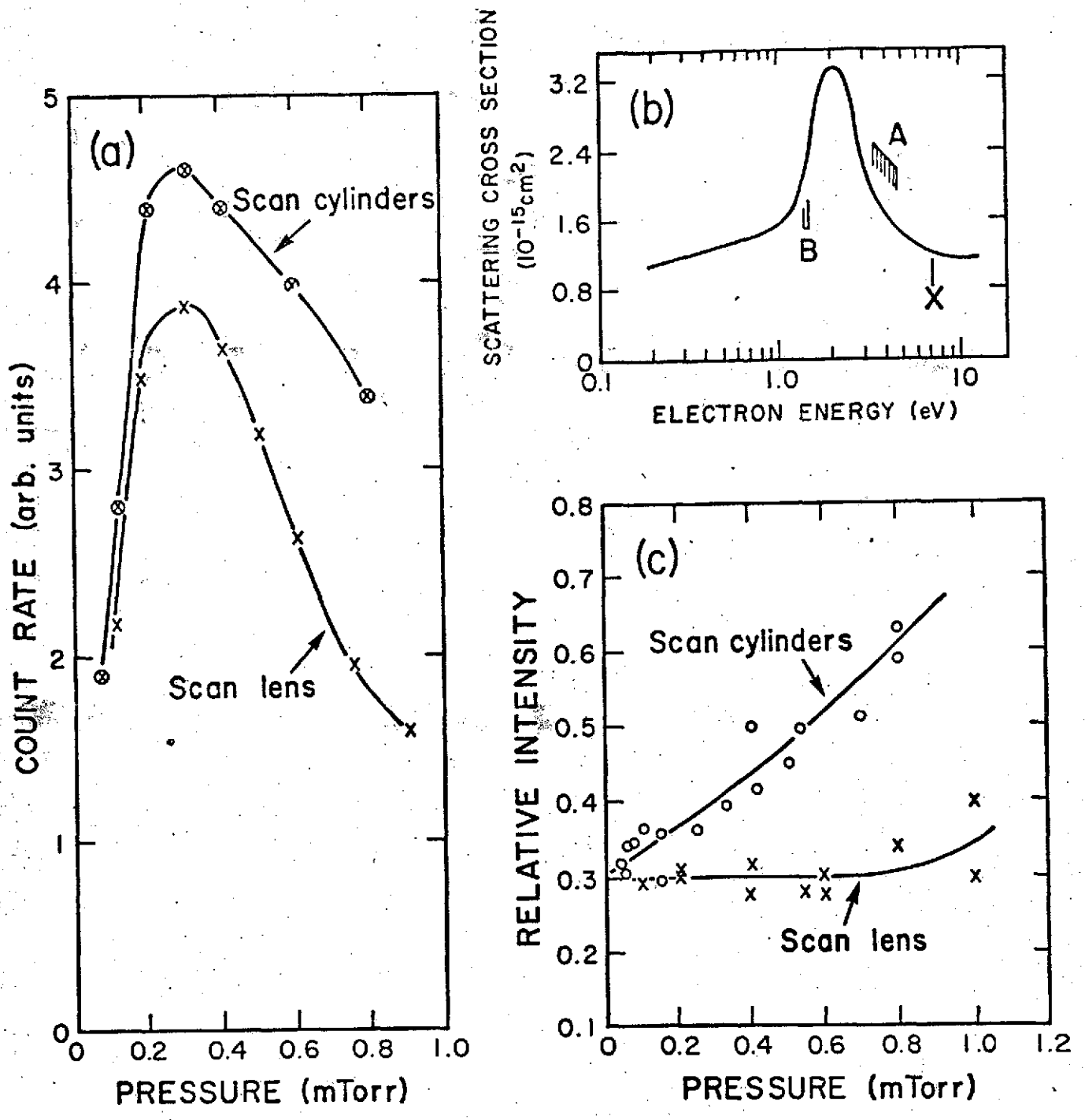

Figure 4. Graphs showing the effects of electron scattering in the analyzer, for the two recording modes. (a) Count rate of CO^+ X $^1\Sigma^+$ v=0 photoelectrons at 58.4 nm as a function of the pressure in the region between the cylinders. (b) CO electron scattering cross section together with the energies of CO photoelectrons at 58.4 nm. (c) Measured intensity ratio of the CO^+ A and B electronic states.

source, dispersed with a ½ m Seya-Namioka monochromator. The rate at which electrons are produced in the ionization chamber, for low gas pressures, is given by

$$\dot{N} = I_o \gamma \sigma n \ell ,$$

where σ is the photoabsorption cross section of the gas, I_o is the photon flux incident on the source of length ℓ, γ is the ionization yield of the gas, and n is the gas particle density. It has been shown that for an analyzer utilising our geometry, the number of electrons per second entering the analyzer is proportional to the solid angle Ω accepted by the entrance slit, independently of the degree of polarization of the radiation and the angular distribution of the ejected electrons about the electric vector.[4] The remaining factors influencing the number of electrons detected are the transmission function of the analyzer and the efficiency of the detector itself for electrons of different energies, including the focussing onto the entrance cone of the multiplier. These two factors may be combined into the term C(E), the collecting efficiency of the analyzer. Thus the rate at which electrons are detected is

$$\dot{N}_d = I_o \gamma \sigma n \ell \Omega C(E) \quad .$$

For the rare gases, γ is a constant equal to unity. If the pressure in the analyzer is constant, n is constant. The source length ℓ and solid angle Ω are fixed by the geometry of the analyzer. Hence at constant pressure,

$$\dot{N}_d \propto I_o \sigma C(E) \quad .$$

C(E) may thus be determined on a relative basis by recording a number of photoelectron spectra from one of the rare gases at a fixed scan rate and at different wavelengths to give different electron energies. If the pressure in the ion source remains constant during the recording, the relative

collecting efficiency is given by $\dot{N}_d/(I_o\sigma)$ at each wavelength. The calibration results for a number of different ion chambers, obtained with a spark discharge source, have been presented elsewhere.[3] The present ion chamber was calibrated with the duoplasmatron light source, which provides radiation continuous in time and consequently electron counting techniques may be utilised. The intensity of the light source was monitored on a calibrated aluminum photocathode at the rear of the ionization region. The photon spectrum was recorded before and after the photoelectron spectra as a check on the stability of the source, with no gas present and a potential of +100 V on the isolated ion chamber with respect to the grounded inner cylinder. The photocathode current, typically 10^{-11} ampere, was measured with a Keithley type 416 picoammeter.

Photoelectron spectra were recorded from both argon and xenon. The relevant cross-sections were taken from the literature.[6] The intensities of the $^2P_{3/2}$ and $^2P_{1/2}$ peaks in argon were summed at each wavelength and the energy was taken as the mean of the peaks, weighted by the 2:1 theoretical statistical weight for 3/2:1/2 spin splitting. For xenon, separate curves were plotted for the $^2P_{3/2}$ and $^2P_{1/2}$ peaks; these were normalized to one another at the higher electron energies. The $^2P_{3/2}$ to $^2P_{1/2}$ intensity ratio in each of the rare gases has been shown to be constant with wavelength.[7] In fact, a plot of the $^2P_{3/2}$ to $^2P_{1/2}$ intensity ratio as measured by the analyzer shows if the collecting efficiency is changing over the energy span of the two peaks.

The data showing the calibration of the present collecting efficiency are plotted in Figure 5, for a pass energy of 3 eV.

The collecting efficiency was monitored as a function of time by periodically recording spectra from oxygen at a wavelength of 73.6 nm (Ne I)

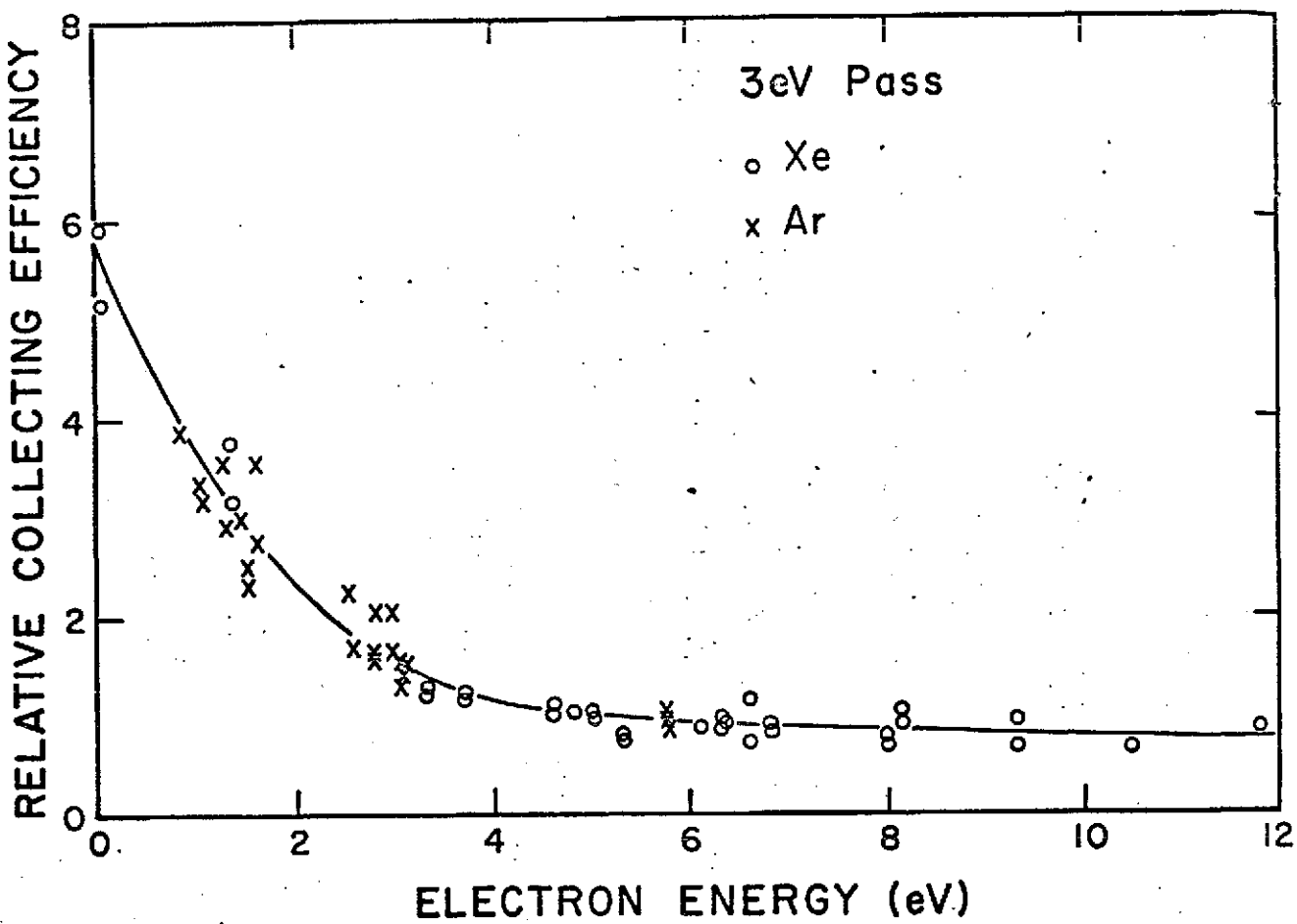

Figure 5. Collecting efficiency of the analyzer for a pass energy of 3 eV.

at a pass energy of 3 eV. A spectrum (for a pass energy of 1.0 eV) is shown in Figure 6. The ground state of O_2^+ is autoionized and vibrational structure up to v=20 is clearly seen. The $^2\Pi$ splitting of 24.2 meV[8] is also resolved in this spectrum. The spectrum provides a source of electrons of reasonable intensity over the energy range 0 to 0.75 eV (the a $^4\Pi$ state of O_2^+) and 1.9 to 4.8 eV (the X $^2\Pi$ state of O_2^+ up to v=14). No significant changes in the relative populations of these levels as detected by the analyzer were noted, indicating that the surfaces of the analyzer, coated with colloidal graphite, did not change sufficiently to affect the results.

The relative collecting efficiency as a function of the electron energy was determined for different pass energies by the cross section method for electron energies greater than 1.5 eV. It was found that the different curves could be normalized to be the same. The oxygen spectrum at 73.6 nm was also used as a check. Collecting efficiencies for spectra recorded at pass energies of 0.75, 1.0, 1.5, 2.0 and 2.5 eV, all relative to that for a pass energy of 3 eV, are plotted in Figure 7. The curves depart only below 0.7 eV, where the analyzer becomes much more sensitive to low energy electrons as the pass energy is lowered, with the sensitivity peaking at about 0.2 eV.

The collecting efficiency for electrons of different energies was also measured by a method based on that of Poole et al.[9] They proposed a technique for measuring the effect of a retarding lens on the transmission of an electron energy analyzer, which is summarized as follows. Photoelectron spectra were recorded from a number of gases at a number of wavelengths. The count rate (for a given primary electron energy) at each wavelength was measured as a function of the pass energy, by varying the degree of acceleration or retardation in the lens. Then the assumption was

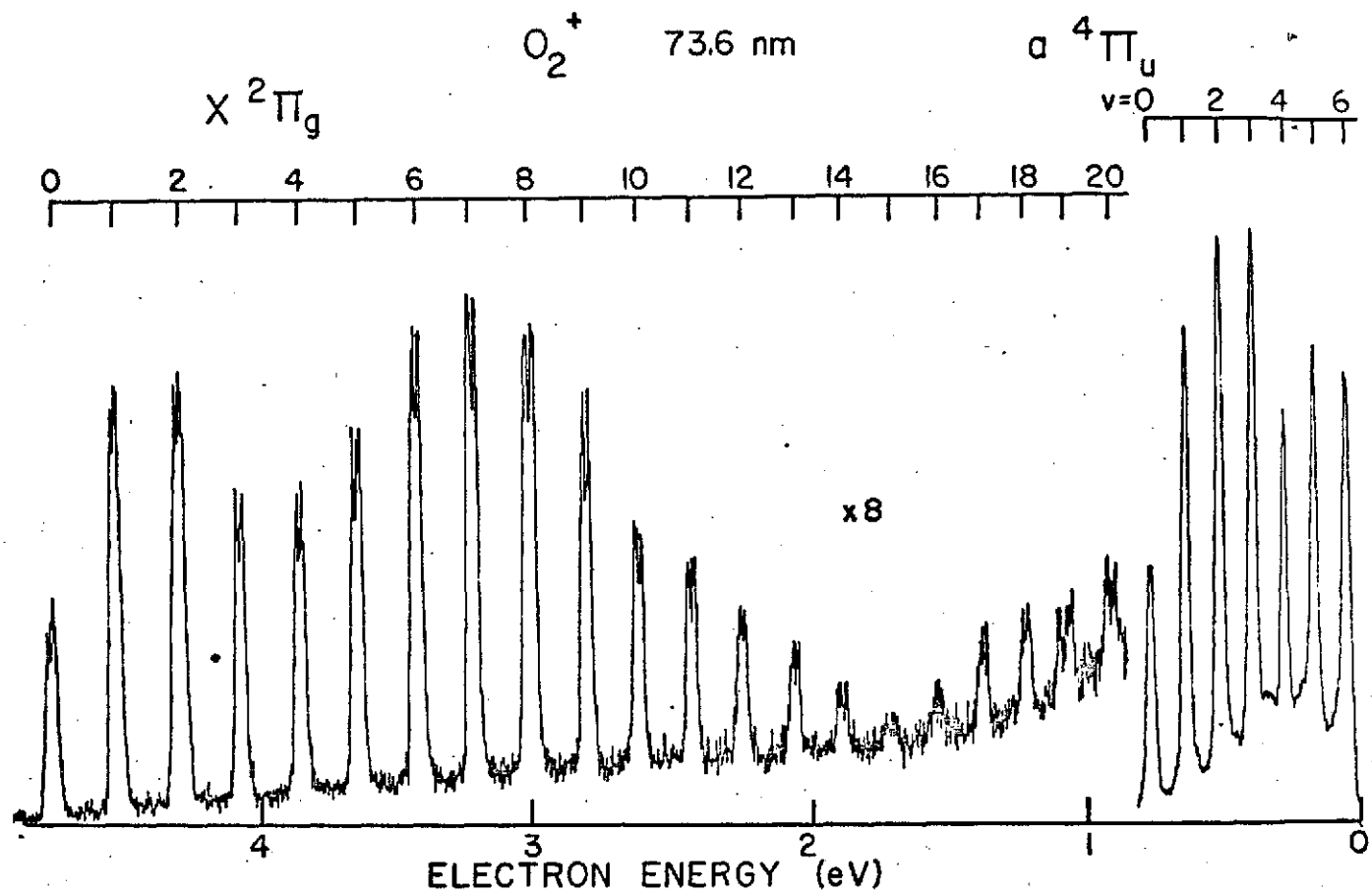

Figure 6. Photoelectron spectrum recorded from oxygen at a wavelength of 73.6 nm with a 1 eV pass energy.

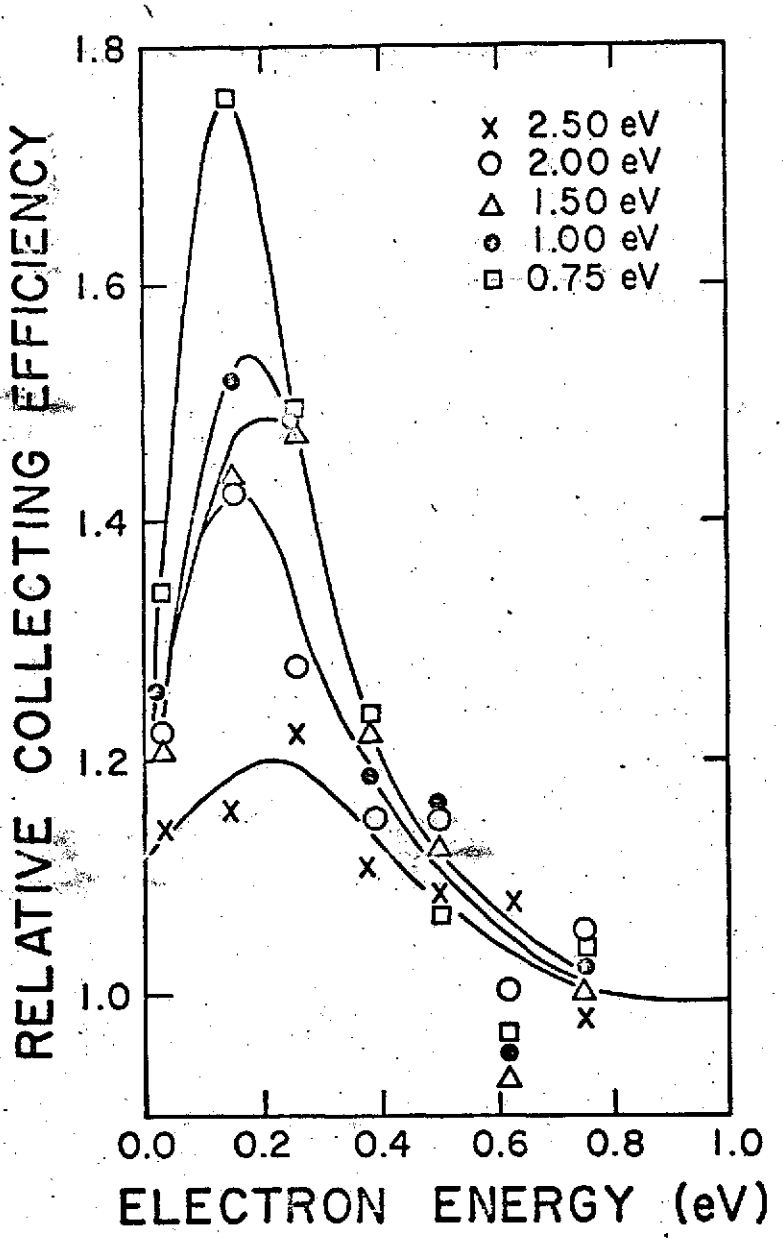

Figure 7. Collecting efficiency of the analyzer for the pass energies listed, relative to that for a pass energy of 3 eV.

made that the transmission of the analyzer was unity when the electrons had zero acceleration in the lens. Thus a family of curves of collecting efficiency *vs.* pass energy for electrons of different energies was generated, all normalized at the point where the pass energy equaled the primary electron energy. The curves were then interpolated to find the collecting efficiency as a function of the electron energy, for a given pass energy. This curve was then used to correct a spectrum recorded at a given pass energy by scanning the voltage on the lens.

The above "pass energy" technique developed by Poole *et al.* for the calibration of their analyzer has been generalized by the present authors. The theory can be expressed analytically without reference to any specific experimental data. To do this it is necessary to make a basic assumption. Namely, that the collecting efficiency C of the analyzer, which is a function of both the kinetic energy of the electrons E_k and the pass energy E_p, may be separated into independent functions of the two variables. That is,

$$C(E_k, E_p) = f(E_k) \cdot g(E_p). \tag{1}$$

The pass energy of the analyzer E_p is the energy of the electron after passing through the accelerating/retarding lens. Thus,

$$E_p = E_k + V_{ar} \quad , \tag{2}$$

where V_{ar} is the variable voltage applied to the accelerating/retarding lens and may be positive or negative.

To evaluate Eq. (1) we consider the collecting efficiency when $E_k = E_p$, that is, when the lens voltage is zero. Equation (1) becomes

$$C(E, E) = f(E) \cdot g(E) \quad . \tag{3}$$

The function f(E) is, therefore, given by

$$f(E) = C(E, E)/g(E) \quad . \tag{4}$$

Inserting Eq. (4) into Eq. (1) we get

$$C(E_k, E_p) = C(E_k, E_k) \cdot g(E_p)/g(E_k). \tag{5}$$

If a spectrum is now analyzed at a fixed pass energy the function $g(E_p)$ will be constant. Therefore,

$$C(E_k, E_p) \propto \frac{C(E_k, E_k)}{g(E_k)} \quad . \tag{6}$$

For Eq. (6) to be useful the functions C(E, E) and g(E) must be known. The forms of the functions are discussed below.

The results of Poole et al. can be achieved quite simply from Eq. (6). They assumed that C(E, E) was a constant. Further, they found experimentally that the function g(E) was proportional to E.[10] Thus, in their case,

$$C(E_k, E_p) \propto \frac{1}{g(E_k)} \propto \frac{1}{E_k} \quad .$$

This is the result obtained for their particular analyzer. If analytical expressions for the functions C(E, E) and g(E) are not available they must be determined experimentally. Determination of C(E, E) is not so straightforward and will be assumed to be constant for the present. The function g(E) is readily measured by plotting a curve of the count rate of photoelectrons from any source, at one wavelength, as a function of the pass energy. (Poole et al. did this for a number of different electron energies. All the curves were straight lines passing through the origin.[9,10])

The present results show g(E) to increase linearly with E then they level off approaching a plateau. The results are plotted in Figure 8 for our

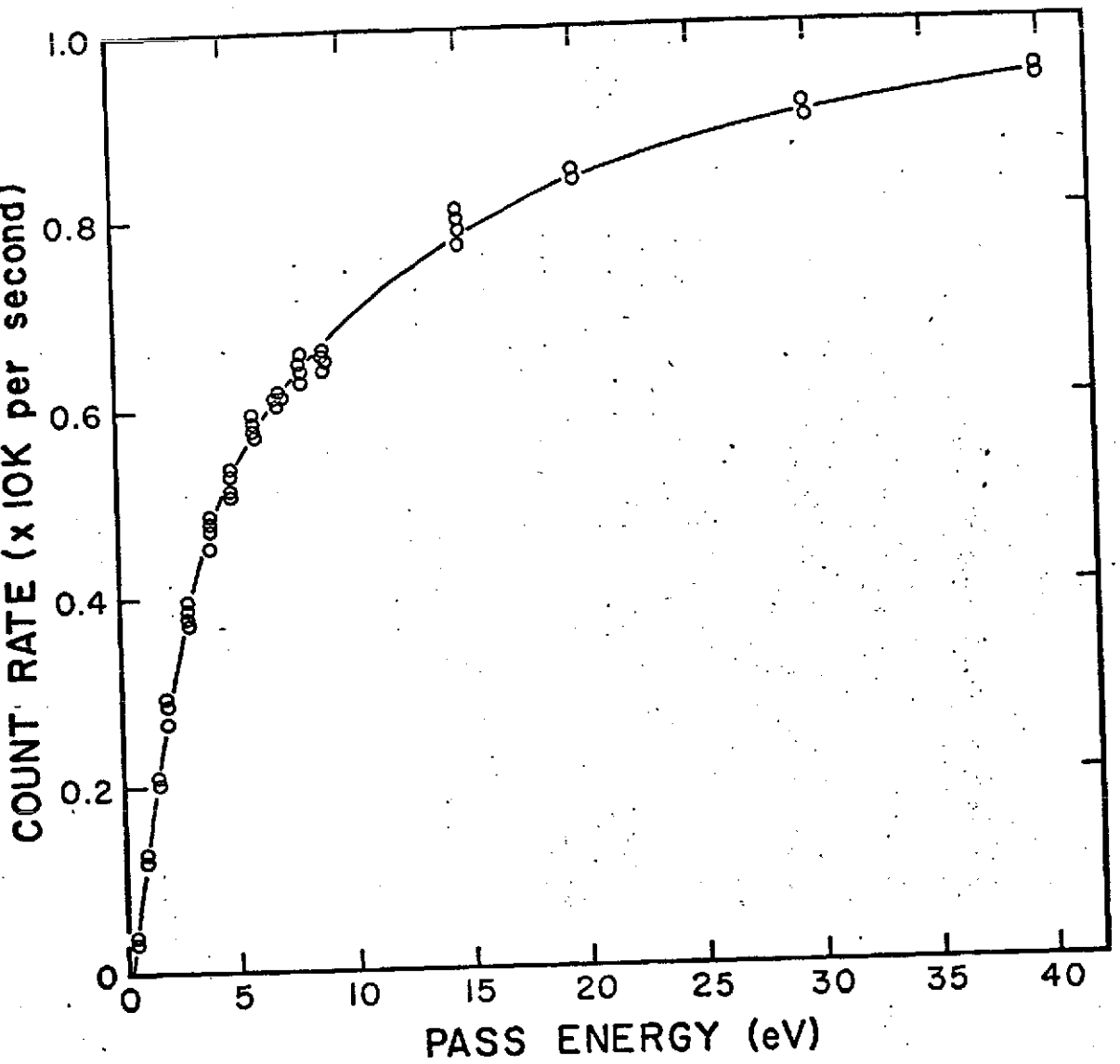

Figure 8. Count rate of xenon photoelectrons at 58.4 nm as a function of the analyzer pass energy.

analyzer. The photoelectrons were produced by ionizing xenon with 58.4 nm radiation. Both the $^2P_{3/2}$ and $^2P_{1/2}$ electrons were used. The electrons were retarded or accelerated to cover the energy range 0 to 40 eV. The two curves were normalized by multiplying the $^2P_{1/2}$ count rate by 1.54; this is the ratio of the $^2P_{3/2}$: $^2P_{1/2}$ states which we had determined previously. The two electron energies are 1.31 eV apart. No significant differences were observed in the normalized data and a single curve was obtained. This curve is inverted in Figure 9, and normalized to the 3 eV pass curve (as determined by the cross section method) at an electron energy of 5 eV. The only significant differences in the results obtained by the two methods occurs at low energies. The deviation between the two methods at low electron energies is caused by the assumption that the function C(E, E) is constant with respect to E. We have shown previously, by the cross section method,[3] that the collecting efficiency of our analyzer with zero potential difference across the lens (i.e. when the spectrum is taken by scanning the voltage across the cylinders and $E_k = E_p$) is not constant, but drops off at low energies. This curve is reproduced in Figure 10. However, the collecting efficiency does become constant above about 4 eV, and it is in this region that excellent agreement occurs between the two methods.

Equation (5) shows that all the collecting efficiency curves obtained at different pass energies should be identical to within a normalizing constant. The cross section method was used to calibrate the collecting efficiency for pass energies of 2 and 4 eV, in addition to the 3 eV curve given above. No significant differences in the normalized curves could be detected over the electron energy range of 2 to 11 eV. As a further check, the photoelectron spectrum of oxygen was recorded at 73.6 nm with a number of different pass energies. Differences between the intensity distributions

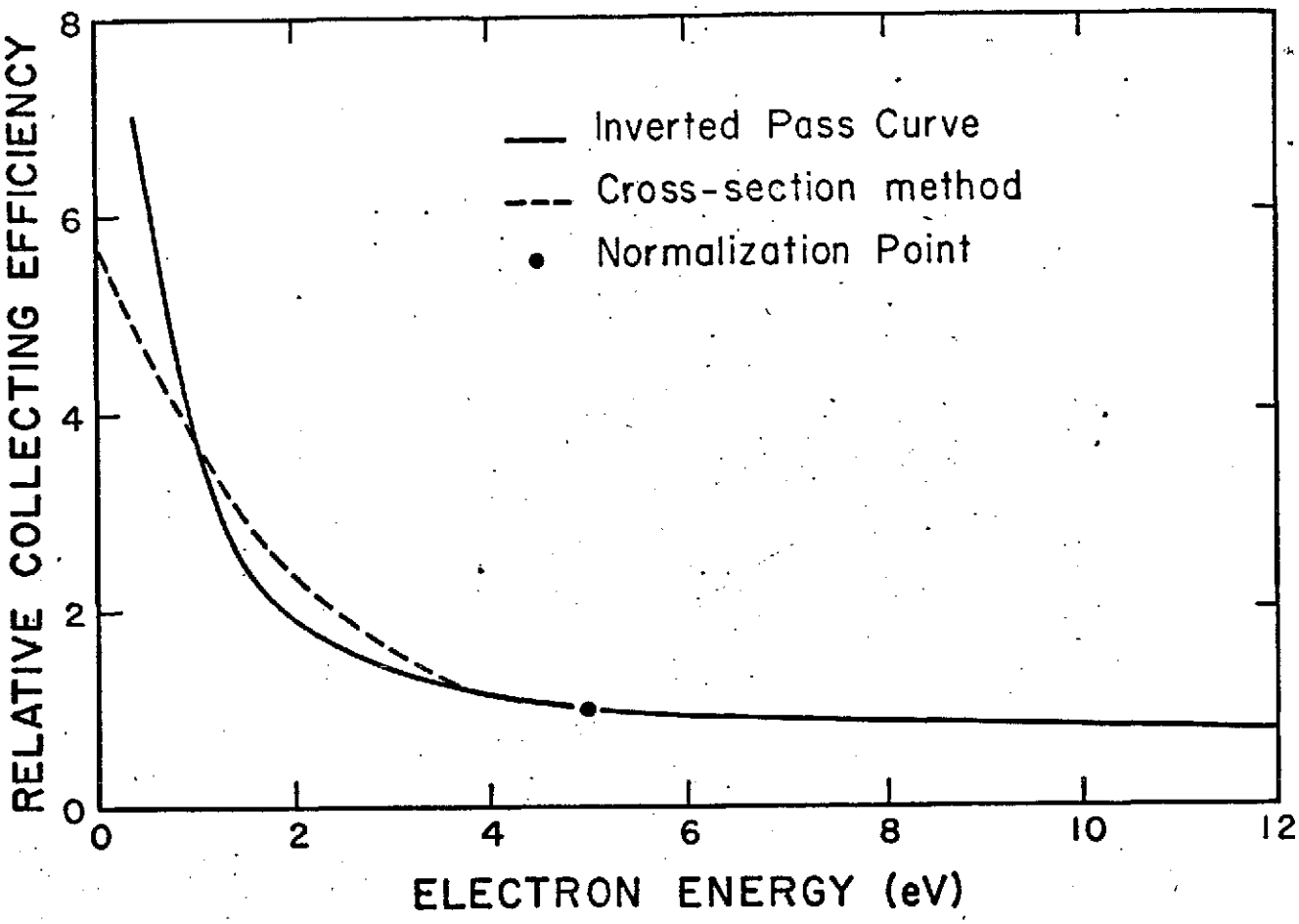

Figure 9. Collecting efficiency obtained by inverting the count rate vs. pass energy curve, compared with that obtained by the cross-section method.

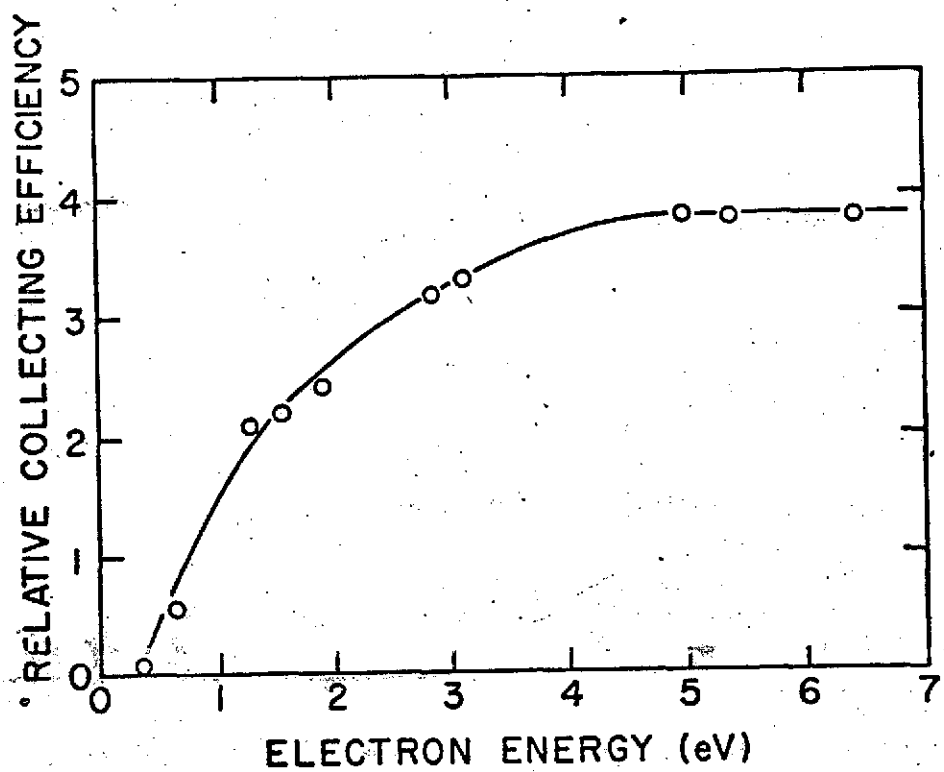

Figure 10. Collecting efficiency of the analyzer for the condition that the pass energy equals the electron energy.

only occurred in the energy range below 0.7 eV (see Figure 7); above this energy, the intensity distributions could be normalized to be identical to within experimental error (± 5%).

The collection efficiency of an analyzer, C(E, E), when $E_k = E_p$ might be expected to be independent of the electron energy and depend solely on the geometry of the analyzer. However, low energy electrons may be discriminated against because of localized contact potentials within the ion chamber and because of residual magnetic fields. Other factors affecting the transmission include the selective scattering of electrons of specific energies. Because $E_k = E_p$ the electrons now traverse the analyzer at different energies, and the path length may be appreciable (18 cm in our case). Thus any structure in the electron scattering cross section over the energy range of interest may produce differential scattering from the residual gas in the deflecting region. Further, the efficiency at the detector itself may be a function of energy, especially if the electrons are focussed into a channeltron by the voltage on the cone and may impact on different regions. The gain of such detectors has been shown to very greatly across the face of the cone.[11] The detector in the present analyzer is placed close to the focal point on the axis, and a 300 V accelerating potential is applied to the cone.

III. RESULTS

Nitrogen

(1) Branching Ratios

Photoelectron spectra were recorded from nitrogen at wavelengths ranging from 74.0 to 52.2 nm. As an example, the 58.4 nm (He I) spectrum is plotted in Figure 11. At each wavelength, the intensities of the observed vibrational peaks were summed after correcting for the collecting efficiency of the analyzer, and the relative intensity that each electronic state appearing in the spectrum contributed to the total was recorded as the branching ratio for that state. The wavelengths of the spectra and the corresponding branching ratios are listed in Table 1. The wavelengths (in nm) and their origin are given as listed by Kelly,[12] rounded to 4 decimal places. Those wavelengths given to 2 decimal places in the table represent an average for those cases where a number of emission lines were included in the bandpass of the monochromator. The best obtainable bandpass was 0.05 nm; in many cases where the emission lines were isolated, the monochromater slits were widened to give an increase in intensity. Times taken to record the spectra ranged from minutes to 1 or 2 days.

At a number of wavelengths, particularly those longer than the threshold for ionization to the B $^2\Sigma_u^+$ state of N_2^+, the effects of autoionization could be seen in the vibrational intensity distributions. The final column in Table 1 indicates whether autoionization was present. A spectrum recorded from nitrogen at a wavelength of 73.6 nm (Ne I) is plotted in Figure 12. The vibrational structure of the X $^2\Sigma_g^+$ state extends up to the A $^2\Pi_u$ state, in contrast to the 58.4 nm spectrum. This 73.6 nm spectrum was recorded with a 0.75 eV pass energy to resolve the X $^2\Sigma_g^+$ v=4 peak from

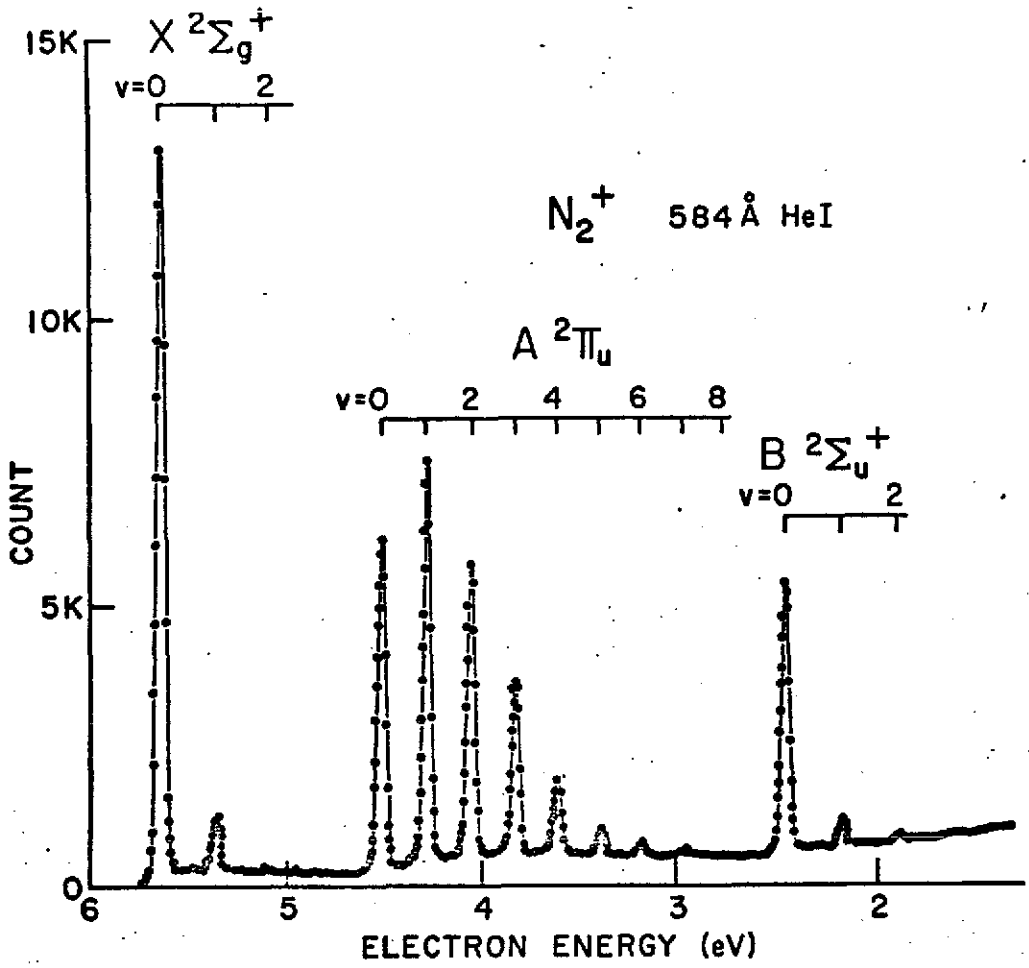

Figure 11. Photoelectron spectrum recorded from nitrogen at a wavelength of 58.4 nm.

Table 1. Photoelectron Branching Ratios for Photoionization of N_2 ($X\ ^1\Sigma_g^+$) to the N_2^+ ($X\ ^2\Sigma_g^+$), ($A\ ^2\Pi_u$) and ($B\ ^2\Sigma_u^+$) states.

Wavelength (nm)	Origin	Branching Ratio (%) $X\ ^2\Sigma_g^+$	$A\ ^2\Pi_u$	$B\ ^2\Sigma_u^+$	
74.0270	Ar II	61.0	39.0		*
73.5895	Ne I	72.9	27.1		*
73.0929	Ar II	50.6	49.4		*
72.5548	Ar II	49.1	50.9		*
72.3361	Ar II	61.5	38.5		*
71.8090	Ar II	31.9	68.1		*
70.4523	Ar II	32.3	67.7		*
69.80	Ar II	35.1	64.9		*
67.7952	Ar II	29.0	71.0		**
67.1852	Ar II	36.6	63.4		**
67.15	N II	32.3	67.7		**
66.4563	Ar II	34.6	65.4		**
66.1869	Ar II	37.6	62.4		**
66.0286	N II	32.4	55.0	12.6	
64.50	N II	34.9	51.4	13.7	
63.7282	Ar III	36.9	51.8	11.3	
61.2372	Ar II	32.6	57.7	9.7	
59.7700	Ar II	33.7	58.6	7.7	
58.4334	He I	37.8	55.1	7.2	

Table 1. Continued.

Wavelength (nm)	Origin	Branching Ratio (%)		
		$X\ ^2\Sigma_g^+$	$A\ ^2\Pi_u$	$B\ ^2\Sigma_u^+$
58.0263	Ar II	35.7	56.2	8.1
57.27	Ar II	36.1	56.6	7.3
56.0223	Ar II	36.7	54.1	9.2
55.62	Ar II	33.2	56.6	10.3
54.0806	Ar II	37.3	53.7	9.0
53.7030	He I	37.6	53.0	9.5
52.2213	He I	38.2	53.2	8.6

* Autoionized structure present

** Weak autoionized structure present

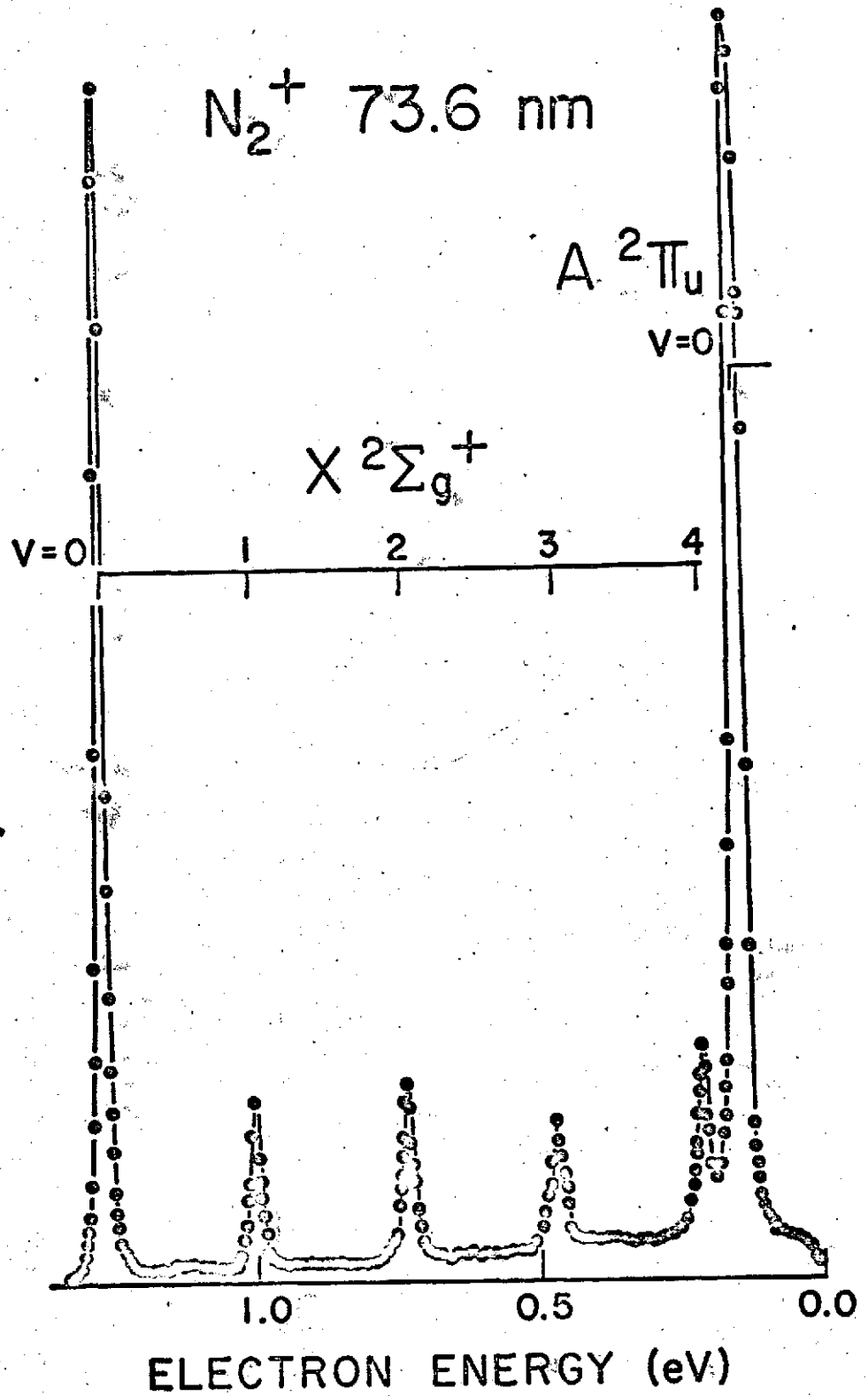

Figure 12. Photoelectron spectrum recorded from nitrogen at a wavelength of 73.6 nm with a 0.75 eV pass energy.

the v=0 peak of the A $^2\Pi_u$ state. The $^2\Pi_u$ state peak is broadened by the 9.3 meV spin orbit splitting of this level.[13]

Table 2 lists the relative vibrational intensities of the X $^2\Sigma_g^+$ state at wavelengths where autoionization was present. A qualitative study of the effects of autoionization has not been attempted here, as the emission lines used may not coincide with the strongest point of the autoionizing resonance.

The branching ratios for the X $^2\Sigma_g^+$, A $^2\Pi_u$ and B $^2\Sigma_u^+$ states are plotted as a function of wavelength in Figure 13. Photoelectron branching ratios have been reported for nitrogen by Blake and Carver for the wavelength range from 74.0 to 58.4 nm. These data were recorded with a Lozier type apparatus, collecting electrons normal to the direction of the photon beam (0.8 nm bandpass from a continuum source) and thus are distorted by changes with wavelength in the polarization of the radiation and the angular distributions of the electrons. The vibrational structure in the photoelectron spectra was also not resolved. Agreement with the present results is poor, probably largely caused by the change in the angular distribution parameter near the ionization threshold, and by the better resolution of the present data.

The rapid changes with decreasing wavelength in the photoionization cross section, caused by autoionization, terminate at the onset of ionization to the B $^2\Sigma_u^+$ state of N_2^+.[15] At shorter wavelengths, the cross section changes fairly smoothly and it is possible to interpolate literature cross sections[16] to the wavelengths at which we recorded photoelectron spectra; the measured branching ratios multiplied by the photoionization cross section then give the partial photoionization cross sections for formation of a specific ionic state. Partial photoionization cross sections for formation

Table 2. Vibrational Intensity Distributions in the ($X\ ^2\Sigma_g^+$) state of N_2^+ at Autoionization Resonances

Wavelength (nm)	Origin	Relative Intensity				
		v=0	v=1	v=2	v=3	v=4
74.51	Ar II	100	32.3	32.1	20.2	11.1
74.3718	Ne I	100	31.8	24.7	16.7	6.9
74.0270	Ar II	100	23.6	15.6	16.6	--
73.5895	Ne I	100	13.7	14.7	10.7	6.8
73.0929	Ar II	100	27.6	6.3	7.7	--
72.5548	Ar II	100	33.7	12.2	14.0	--
72.3361	Ar II	100	47.3	14.3	7.0	--
71.8090	Ar II	100	19.0	12.3	11.9	--
70.4523	Ar II	100	28.7	19.7	--	--
69.80	Ar II	100	13.0	10.3	8.5	--

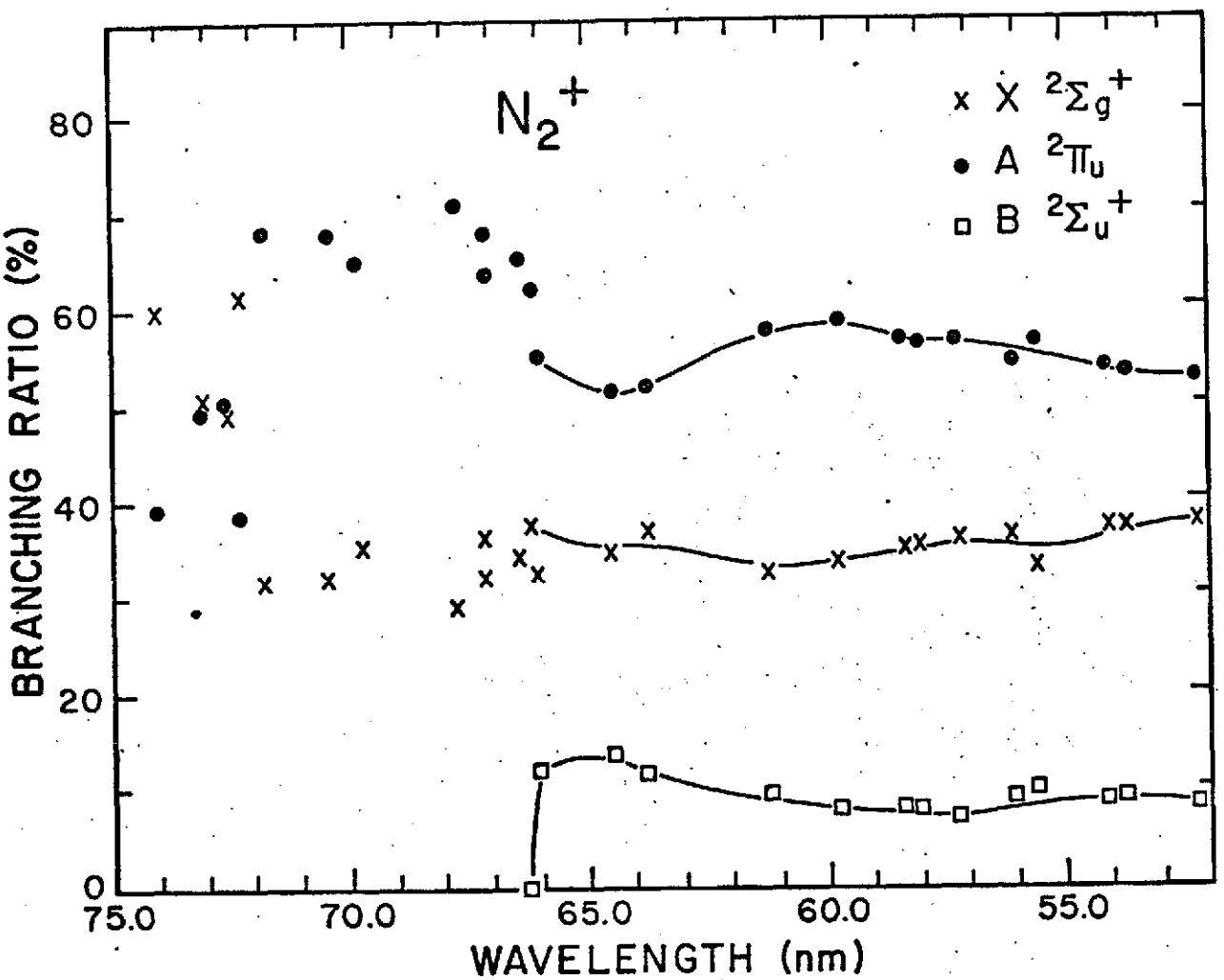

Figure 13. Branching ratios for photoionization of nitrogen to the ionic states listed.

of the N_2^+, $X\ ^2\Sigma_g^+$, $A\ ^2\Pi_u$ and $B\ ^2\Sigma_u^+$ states at wavelengths ranging from 66.0 to 52.2 nm are listed in Table 3 and plotted in Figure 14. Also plotted in Figure 14 are the partial photoionization cross sections for the N_2^+ $B\ ^2\Sigma_u^+$ state as measured by the study of the fluorescent radiation emitted by the $B\ ^2\Sigma_u^+$ state as it decays.[17] Agreement with the present results is seen to be good. Theoretical continuum photoionization cross sections have been calculated for nitrogen by Tuckwell.[18] The agreement with the present results is reasonable for the $X\ ^2\Sigma_g^+$ state, poor for the $^2\Pi_u$ state and for the $B\ ^2\Sigma_u^+$ state the shape of the theoretical curve agrees fairly well, although the magnitude is about a factor of 3 too high..

(2) Continuum Vibrational Intensity Distributions

A number of photoelectron spectra were recorded at wavelengths of 58.4 and 53.7 nm (He I) to determine the vibrational intensity distributions for continuum photoionization from the N_2 $X\ ^1\Sigma_g^+$ (v=0) level to each of the $X\ ^2\Sigma_g^+$, $A\ ^2\Pi_u$ and $B\ ^2\Sigma_u^+$ ionic states. The spectra were recorded at a resolution of 45 meV for sufficient time to show up the weaker members of the vibrational series, which could be safely ignored in determining the branching ratios for the electronic states. The pressure in the analyzer was maintained at less than 0.1 m Torr to reduce pressure sensitive scattering effects. The relative vibrational intensities were corrected for the analyzer transmission and the results of a number of spectra were averaged. In recording the averages, the $X\ ^2\Sigma_g^+$ and $B\ ^2\Sigma_u^+$ distributions, dominated by the v=0 level, were normalized to 100 at this level. The individual $A\ ^2\Pi_u$ state distributions were normalized to have the same sum, then averaged and the averages were renormalized to 100 at the v=1 level.

Up to 15 spectra were averaged to give the distributions shown in

Table 3. Partial Cross Sections For Photoionization of N_2 ($X\ ^1\Sigma_g^+$) to the N_2^+ ($X\ ^2\Sigma_g^+$), ($A\ ^2\Pi_u$) and ($B\ ^2\Sigma_u^+$) states

Wavelength (nm)	Origin	Cross Section ($\times 10^{-18}$ cm^2)			
		Total*	$X\ ^2\Sigma_g^+$	$A\ ^2\Pi_u$	$B\ ^2\Sigma_u^+$
66.0286	N II	23.3	7.5	12.8	2.9
64.50	N II	23.4	8.2	12.0	3.2
63.7282	Ar III	23.4	8.6	12.1	2.6
61.2372	Ar II	23.3	7.6	13.4	2.3
59.7700	Ar II	23.0	7.6	13.6	1.8
58.4334	He I	23.1	8.2	13.0	1.9
58.0263	Ar II	23.0	8.2	12.9	1.9
57.27	Ar II	22.8	8.2	12.9	1.7
56.0223	Ar II	23.1	8.5	12.5	2.1
55.62	Ar II	23.3	7.7	13.1	2.4
54.0806	Ar II	24.2	9.0	13.0	2.2
53.7030	He I	24.4	9.2	12.9	2.3
52.2213	He I	25.0	9.6	13.3	2.2

* Interpolated from data of reference 16.

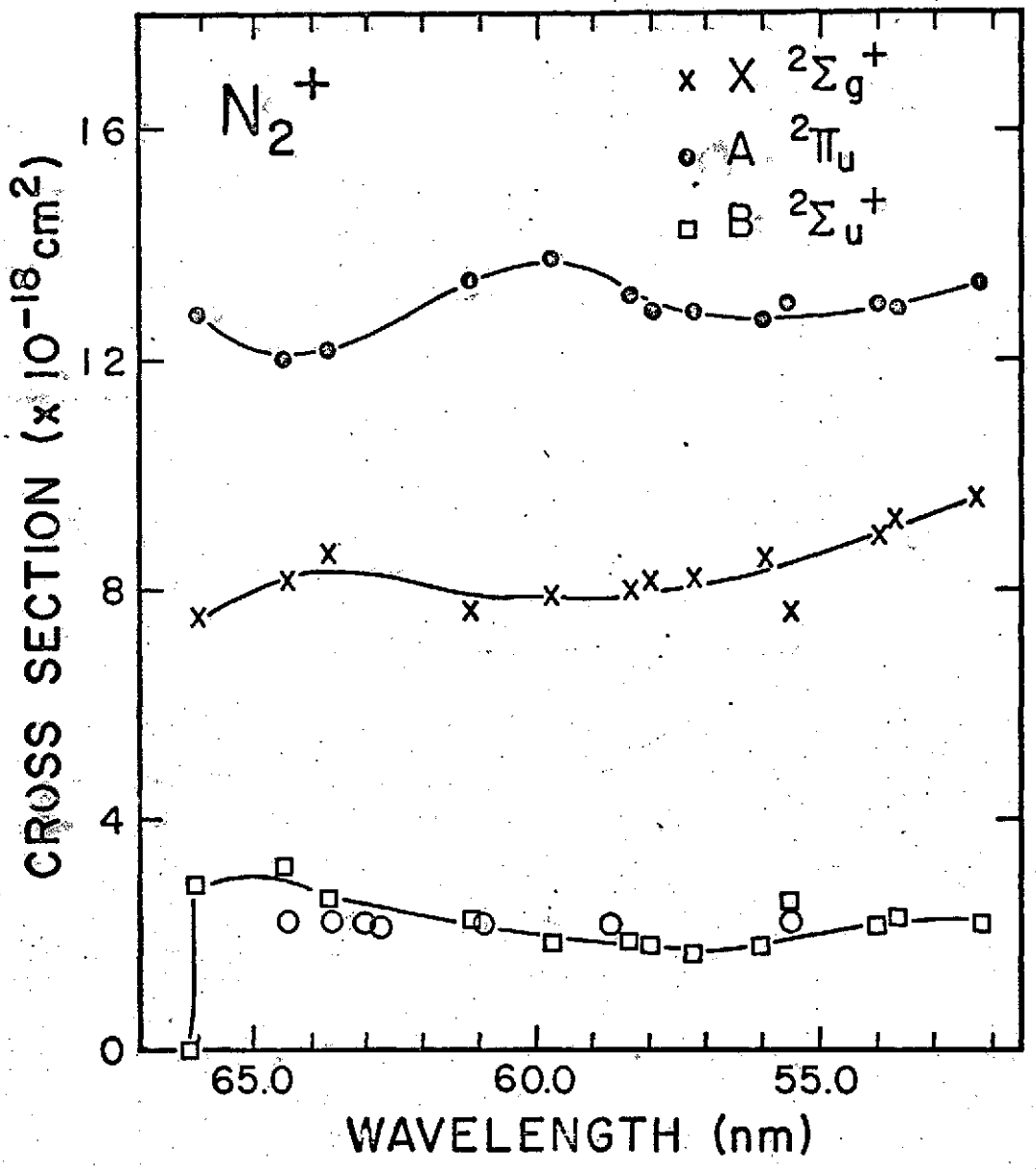

Figure 14. Partial photoionization cross sections for producing the N_2^+ states listed. The data points o are the B-X fluorescence cross sections from ref. 17.

Table 4, along with theoretical Franck-Condon factors for the transitions involved.[19] The errors represent RMS statistical errors in the count rates only. The results for the B $^2\Sigma_u^+$ state include only 53.7 nm spectra as anomalous pressure sensitive distributions, caused by resonant scattering through negative ion states,[20] were observed in all the 58.4 nm spectra in the energy range covered by the B $^2\Sigma_u^+$ transitions. This was true even at the lowest useable pressures in the analyzer. The results for the X $^2\Sigma_g^+$ and A $^2\Pi_u$ ionic states include both 58.4 and 53.7 nm spectra, thus minimizing errors in the determination of the transmission through the analyzer as a function of the electron energy. The error in the transmission calibration could be as high as 15% across the energy range covered by the A $^2\Pi_u$ electrons at each wavelength. No significant differences were noted in the distribution at the two wavelengths.

The N_2^+ vibrational intensity distributions, divided by the Franck-Condon factors, are plotted in Figure 15, normalized to unity at the strongest peak in each band. The A $^2\Pi_u$ and B $^2\Sigma_u^+$ distributions are reasonably well explained by the Franck-Condon factors (apart from the v=7 level of the A $^2\Pi_u$ state). A consistent deviation is seen about the v=4 level of the A $^2\Pi_u$ state. This trend may be explicable by the variation of the electronic transition moment with the internuclear separation of the atoms and/or with the variation in the energy of the emitted electron, as in the case of hydrogen.[21]

The vibrational intensities for the X $^2\Sigma_g^+$ state do not agree with the Franck-Condon factors. The v=1 to v=0 ratio presented here agrees well with the ratio determined by Carlson[22] at 54°44', the angle to the photon beam at which the present analyzer collects electrons. Carlson also found that the v=1 to v=0 ratio at 58.4 nm was dependent on the angle of detection;

Table 4. Vibrational Intensity Distributions and Franck-Condon Factors for Continuum Photon-ionization of $N_2(X\ ^1\Sigma_g^+)$

N_2^+ State	v	Experimental Intensity	FCF[19]
$X\ ^2\Sigma_g^+$	0	100.0	100.0
	1	6.94 ± 0.66	9.27
	2	0.32 ± 0.21	0.59
$A\ ^2\Pi_u$	0	87.1 ± 3.1	84.9
	1	100.0 ± 2.8	100.0
	2	76.3 ± 1.5	68.0
	3	43.5 ± 2.9	35.3
	4	19.1 ± 2.4	15.7
	5	7.09 ± 0.77	6.37
	6	2.51 ± 0.40	2.43
	7	1.70 ± 0.34	0.89
	8	0.37 ± 0.17	0.32
$B\ ^2\Sigma_u^+$	0	100.0	100.0
	1	9.84 ± 2.51	13.1
	2	0.76 ± 0.94	0.25

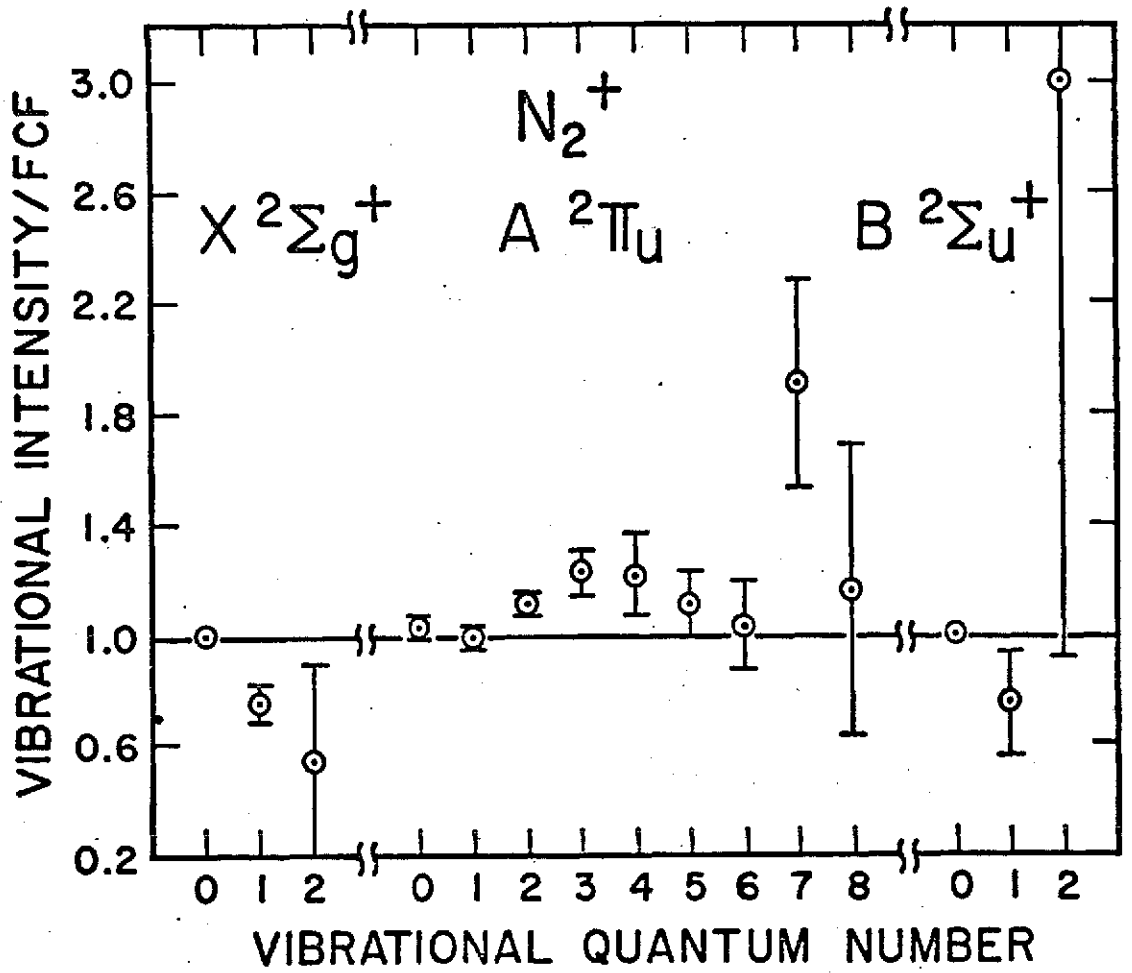

Figure 15. Vibrational intensity distributions for continuum photoionization of nitrogen.

no other electronic states of diatomic molecules have been reported to show angular effects within the vibrational distribution when autoionization is not present. We also measured the v=1 to v=0 ratio for continuum ionization to the N_2^+ X $^2\Sigma_g^+$ state at other wavelengths ranging up to 64.5 nm. All results agreed with the 58.4 nm value, indicating that the anomaly is not confined to 58.4 nm.

Carbon Monoxide

(1) Branching Ratios

Photoelectron spectra were recorded from CO at wavelengths ranging from 74.5 to 52.2 nm. The 58.4 nm (He I) spectrum, uncorrected for the analyzer's collecting efficiency, is plotted in Figure 16. Branching ratios for the electronic states energetically accessible at each wavelength are listed in Table 5 and plotted in Figure 17. As in the case of nitrogen, wavelengths rounded to 2 decimal places indicate that more than one emission line was included in the bandpass of the monochromator.

Autoionization was observed at a number of wavelengths; these are indicated in Table 5. A spectrum recorded at 73.6 nm (Ne I) at a pass energy of 3 eV is plotted in Figure 18. The vibrational population of the X $^2\Sigma^+$ ionic state is clearly seen up to v=9, in contrast to the 58.4 nm spectrum of Figure 16. The low energy region of the 73.6 nm spectrum was re-recorded at a pass energy of 0.75 eV, and the result is plotted in Figure 19. The v=11 level of the ground state is clearly present, and the doublet splitting of the A $^2\Pi_i$ state (spin-orbit splitting of 14.6 meV) is clearly resolved. The autoionized ground state vibrational intensity distributions, corrected for the analyzer transmission, are tabulated in Table 6.

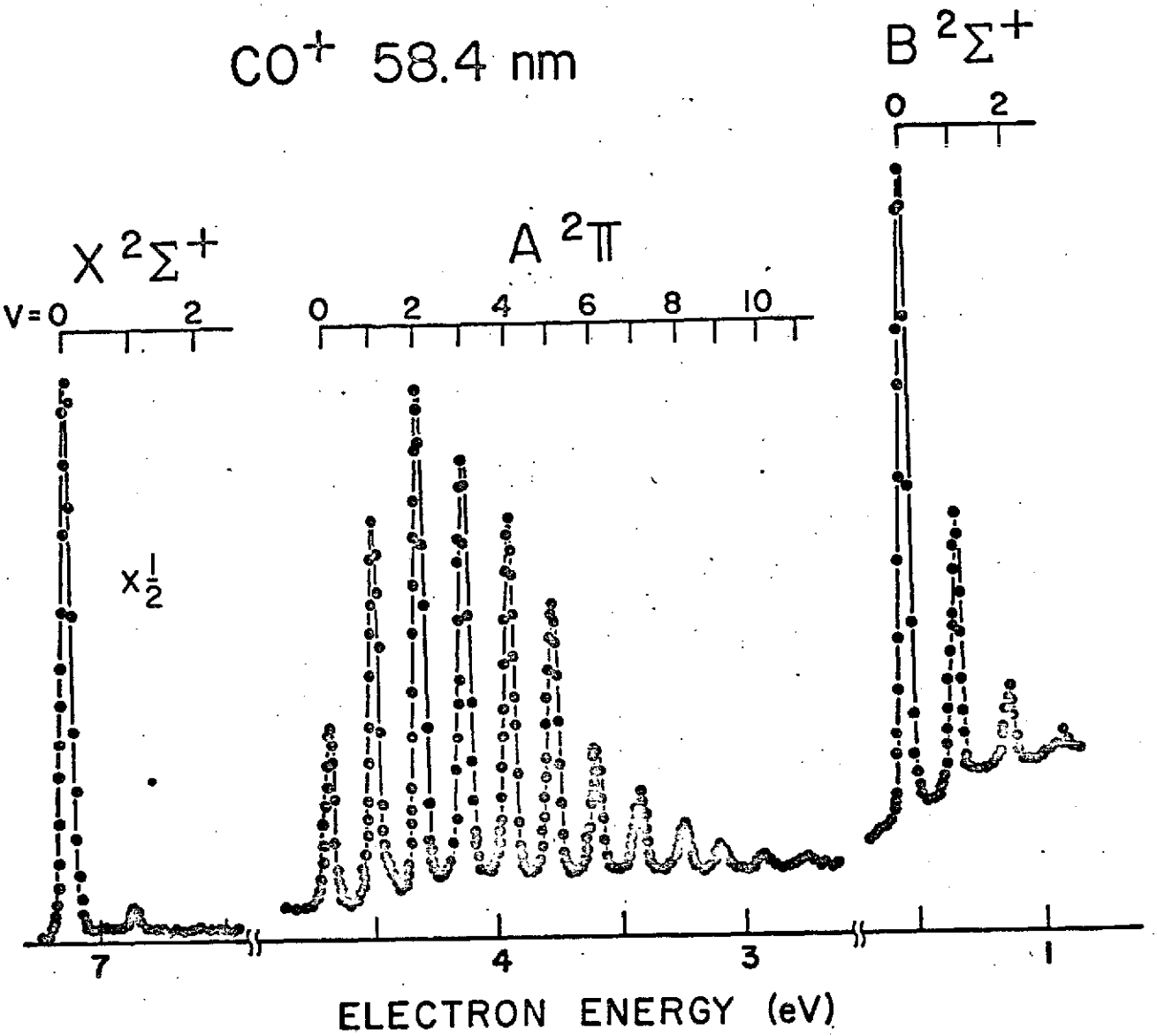

Figure 16. Photoelectron spectrum recorded from carbon monoxide at a wavelength of 58.4 nm.

Table 5. Photoelectron Branching Ratios for Photoionization of $CO(X\ ^1\Sigma^+)$ to the CO^+ $(X\ ^2\Sigma^+)$, $(A\ ^2\Pi)$ and $(B\ ^2\Sigma^+)$ states.

Wavelength (nm)	Origin	Branching Ratio (%) $X\ ^2\Sigma^+$	$A\ ^2\Pi$	$B\ ^2\Sigma^+$	
74.51	Ar II	81.5	18.5		*
74.3718	Ne I	88.4	11.6		*
74.0270	Ar II	59.6	40.4		*
73.5895	Ne I	68.9	31.1		*
73.0929	Ar II	52.0	48.0		**
72.5548	Ar II	46.4	53.6		*
72.3361	Ar II	40.9	59.1		**
71.8090	Ar II	41.4	58.6		**
70.4523	Ar II	40.8	59.2		
69.80	Ar II	43.8	56.2		**
67.7952	Ar II	39.4	59.6		
67.1852	Ar II	44.3	55.7		**
67.15	N II	38.4	61.6		**
66.4563	Ar II	49.1	50.9		
66.1869	Ar II	44.6	55.4		
64.50	N II	40.5	59.5		
63.7282	Ar III	41.7	58.3		
62.93	N II	39.1	54.7	6.2	
61.2372	Ar II	37.1	53.7	9.3	

Table 5. Continued

Wavelength (nm)	Origin	Branching Ratio (%)		
		$X\ ^2\Sigma^+$	$A\ ^2\Pi$	$B\ ^2\Sigma^+$
59.7700	Ar II	34.4	58.0	7.7
58.4334	He I	33.9	57.4	8.7
58.0263	Ar II	28.6	63.2	8.3
57.27	Ar II	31.9	60.7	7.4
56.0223	Ar II	34.9	56.5	8.6
53.7030	He I	37.0	52.6	10.4
52.2213	He I	36.8	53.9	9.3

* Autoionized structure present.

** Weak autoionized structure present.

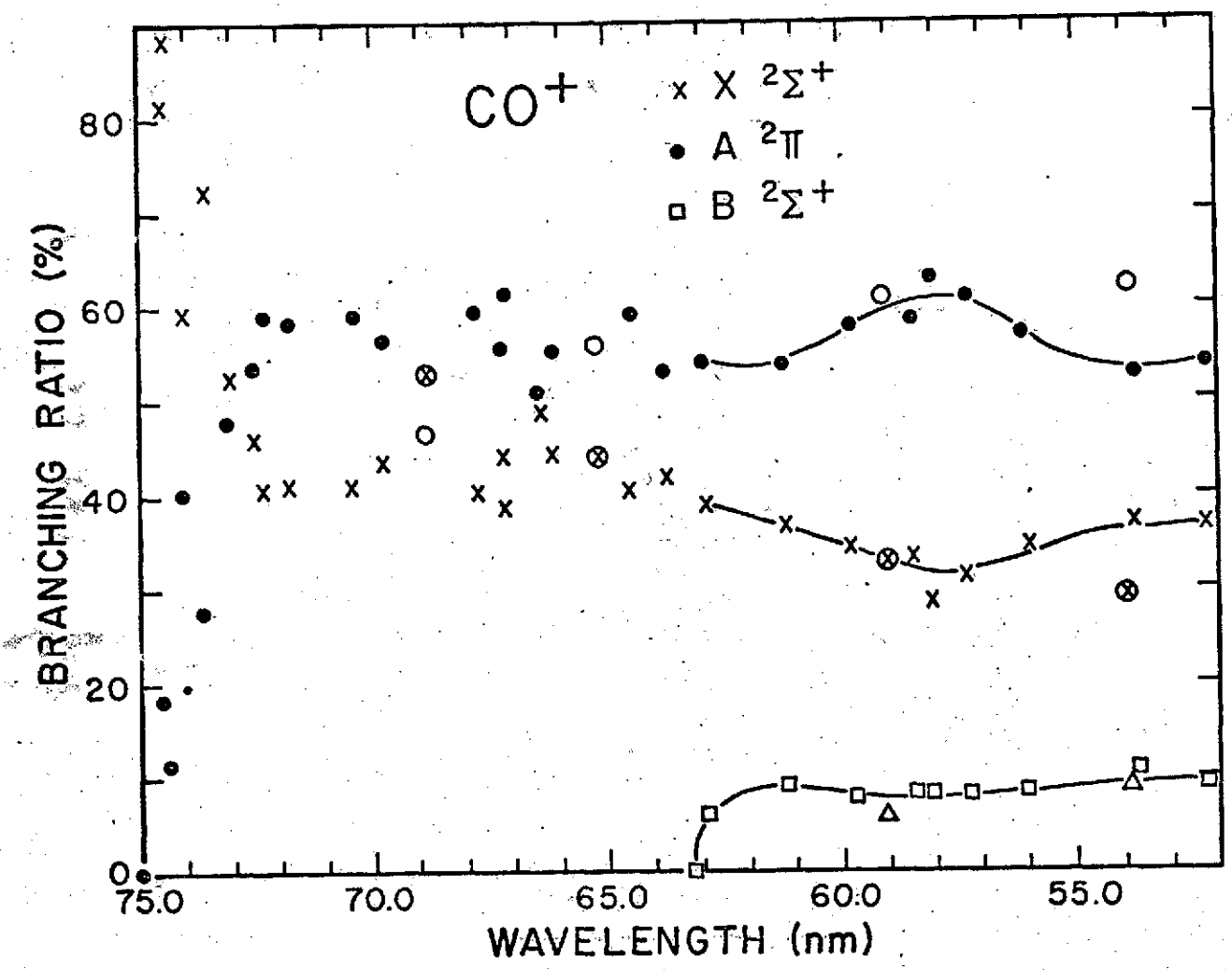

Figure 17. Branching ratios for photoionization of CO to the ionic states listed. The data points ⊗, o and Δ are for production of the CO^+ X, A and B states respectively from ref. 23.

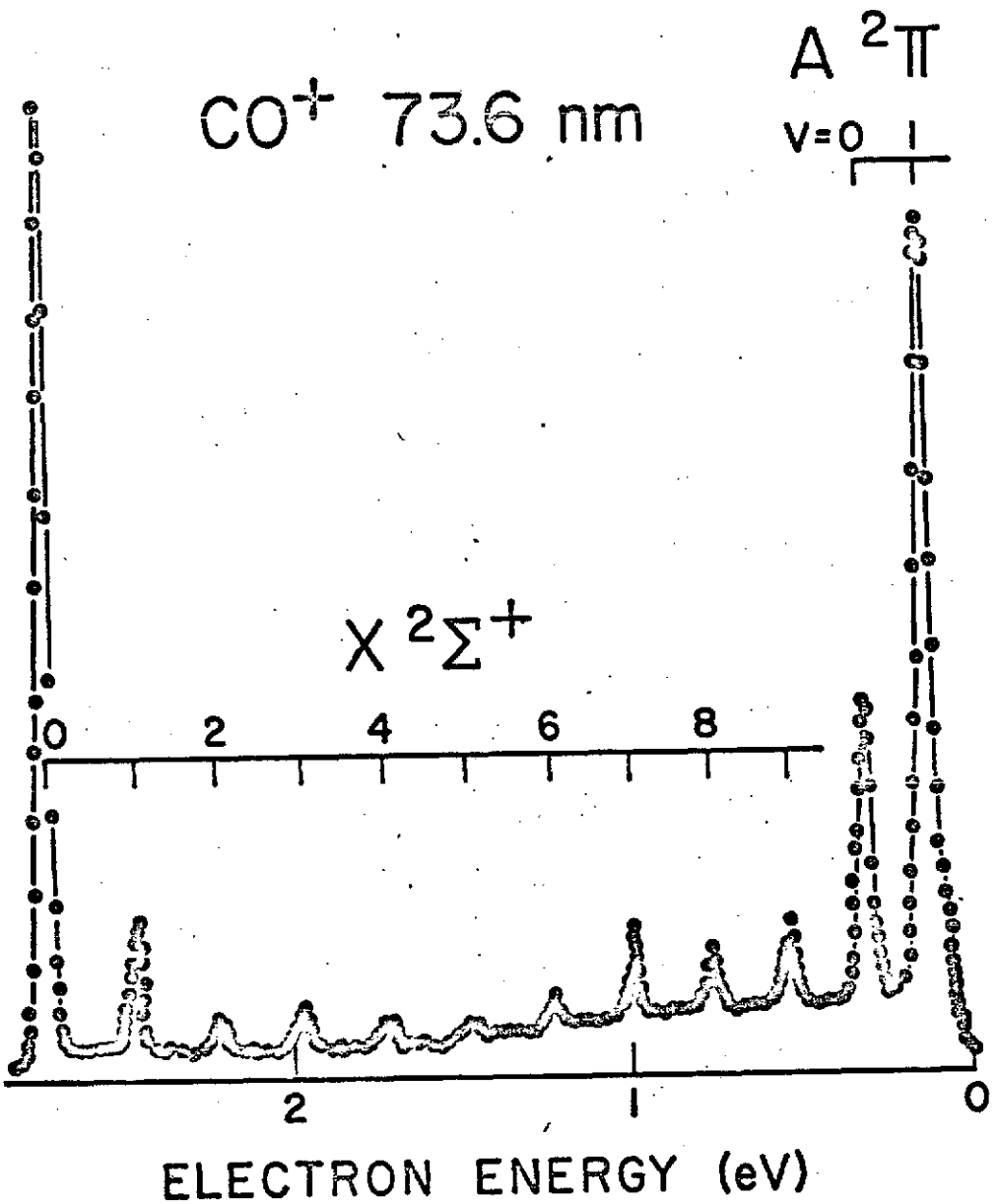

Figure 18. Photoelectron spectrum recorded from carbon monoxide at a wavelength of 73.6 nm.

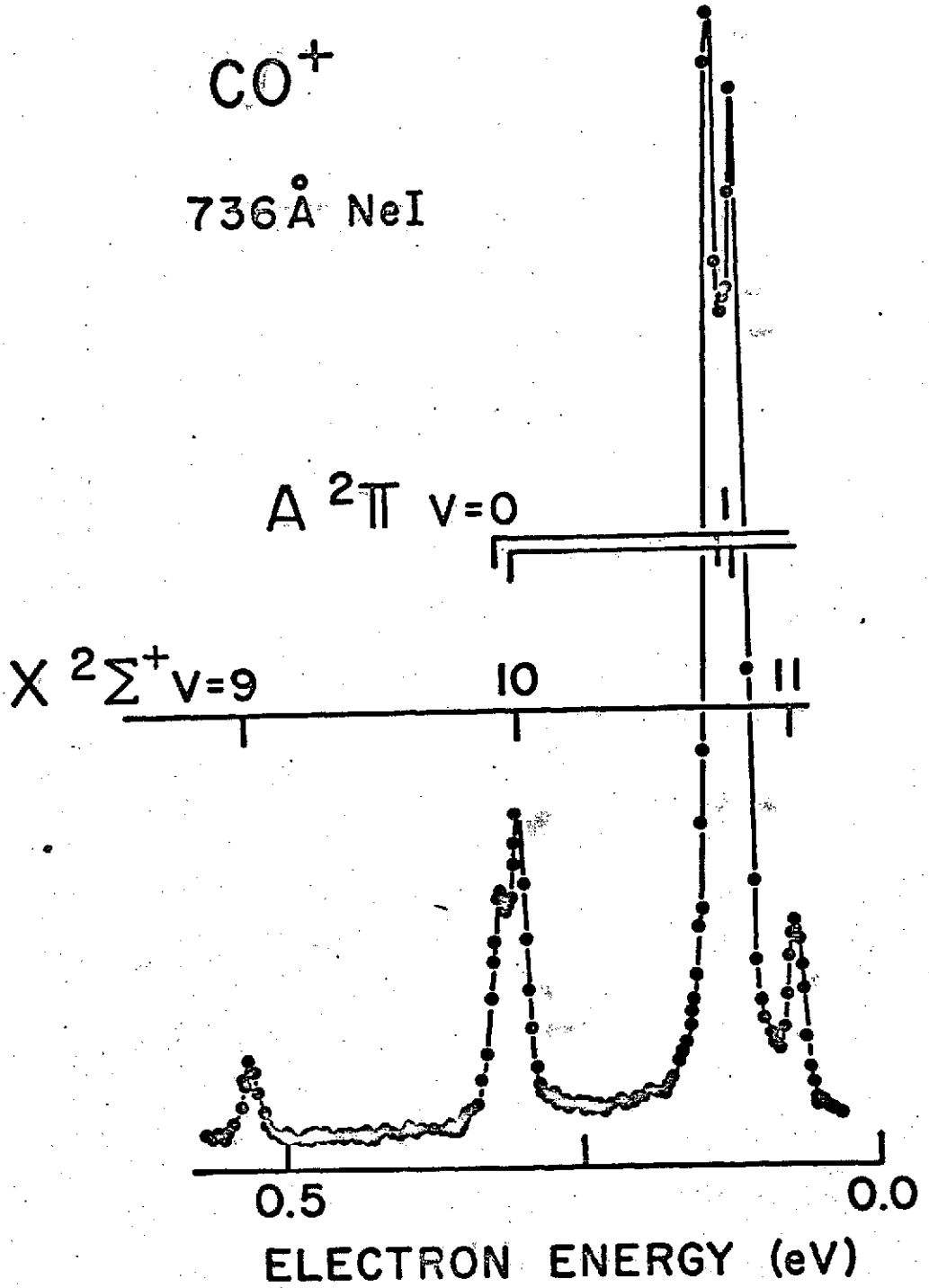

Figure 19. Low energy region of the 73.6 nm photoelectron spectrum from carbon monoxide, taken at high resolution.

Table 6. Vibrational Intensity Distributions in the ($X\ ^2\Sigma^+$) State of CO^+ at Autoionization Resonances.

Wavelength (nm)	Origin	Relative Intensity											
		v=0	1	2	3	4	5	6	7	8	9	10	11
74.51	Ar II	100	19.1	5.6	6.2	10.1	5.6	15.3	10.8	9.1	11.9	--	
74.3718	Ne I	100	6.7	3.6	2.2	4.1	3.2	3.8	3.1	3.6	2.4	--	
74.0270	Ar II	100	16.3	6.2	5.9	8.7	9.3	12.8	9.3	9.4	8.6	--	
73.5895	Ne I	100	12.4	2.7	3.6	1.9	1.3	2.1	4.1	2.7	3.5	--	2.6
72.5548	Ar II	100	39.4	21.6	8.3	3.9	4.2	6.2	3.2	8.9	3.8	--	---

Included in Figure 17 are the branching ratios reported by Van der Weil and Brion.[23] These data were recorded from 10 keV electron impact experiments, measuring energy loss spectra in the forward direction. Under these conditions, dipole transitions dominate the scattering process and the transition rates may be compared with photon impact data at the same energy transfer. The data of Van der Weil and Brion depends on the asymmetry parameter β, which is known at 58.4 nm.[24] Thus their data were corrected for β at 58.4 nm and the agreement with the present results is good at that wavelength. Agreement is worse at wavelengths near 69.0 nm, where the branching ratios depend on the bandpass because of autoionization, and the $X\ ^2\Sigma^+$ and $A\ ^2\Pi_i$ points also differ from the present results at shorter wavelengths than 58.4 nm.

Branching ratios for photoionization of CO have also been reported by Bahr et al.[25] The results agree with the present results within about 30%, with larger discrepancies near the thresholds of the ionic states. Their results were recorded at a bandpass of 0.8 nm with a spherical grid retarding system sampling electrons normal to the photon beam and thus depend on the polarization of the radiation and the angular distribution of the electrons.

At wavelengths shorter than about 68.0 nm, the CO photoabsorption cross section[26] does not show much structure due to autoionization and thus may be reasonably interpolated to the wavelengths at which photoelectron branching ratios were recorded. The photoionization yield has not been measured over much of this region, but can be reasonably assumed to be unity, and the photoionization cross section can be taken to be equal to the photoabsorption cross section. Partial photoionization cross sections deduced from the product of the interpolated photoabsorption cross sections[27]

and the branching ratios given above are listed in Table 7 and plotted in Figure 20. Also plotted in the Figure are the partial cross sections for photoionization to the CO^+ A $^2\Pi_i$ and B $^2\Sigma^+$ states measured by Judge and Lee from fluorescence studies.[28] Agreement is seen to be reasonable for the B $^2\Sigma^+$ state, but the fluorescence values for the A $^2\Pi_i$ state are lower than the present results.

(2) Continuum Vibrational Intensity Distributions

A number of photoelectron spectra were recorded from CO at wavelengths of 58.4 and 53.7 nm (He I) to determine the vibrational intensity distribution for photoionizing transitions from CO X $^1\Sigma^+$ (v=0) to each of the X $^2\Sigma^+$, A $^2\Pi_i$, and B $^2\Sigma^+$ electronic states of CO^+. The experimental details are the same as those discussed in the case of the nitrogen vibrational intensity distributions. The vibrational distributions over the ionic states are listed in Table 8 along with theoretical Franck-Condon factors.[18] As in the case of N_2, the B $^2\Sigma^+$ distribution includes only 53.7 nm spectra, while the X $^2\Sigma^+$ and A $^2\Pi_i$ results are derived from 58.4 and 53.7 nm spectra, with no significant differences observed between the two wavelengths.

The CO^+ vibrational intensities, divided by the Franck-Condon factors, are plotted in Figure 21, normalized to unity at the strongest peak in each band. It can be seen that the X $^2\Sigma^+$ and B $^2\Sigma^+$ distributions are well explained by the Franck-Condon factors, and that the A $^2\Pi_i$ distribution deviates consistently higher than the Franck-Condon factors as the vibrational quantum number increases. As in the case of H_2, this deviation may be explicable by the variation of the electronic transition moment with both the energy of the emitted electron and/or the internuclear separation of the atoms.[21]

Table 7. Partial Cross Sections for Photoionization of CO ($X\ ^1\Sigma^+$) to the CO^+ ($X\ ^2\Sigma^+$), ($A\ ^2\Pi$) and ($B\ ^2\Sigma^+$) States.

Wavelength (nm)	Origin	Cross-section (x 10^{-18} cm^2)			
		Total*	$X\ ^2\Sigma^+$	$A\ ^2\Pi$	$B\ ^2\Sigma^+$
67.7952	Ar II	22.1	8.8	13.3	
67.1852	Ar II	22.2	9.8	12.4	
67.15	N II	22.1	8.5	13.6	
66.4563	Ar II	22.2	10.9	11.3	
66.1869	Ar II	22.2	9.9	12.3	
64.50	N II	22.3	9.0	13.3	
63.7282	Ar III	22.3	9.3	13.0	
62.93	N II	22.3	8.7	12.2	1.4
61.2372	Ar II	22.4	8.3	12.0	2.1
59.7700	Ar II	22.6	7.8	13.1	1.7
58.4334	He I	22.6	7.7	13.0	2.0
58.0263	Ar II	22.6	6.5	14.3	1.9
57.27	Ar II	22.5	7.2	13.7	1.7
56.0223	Ar II	22.5	7.9	12.7	1.9
53.7030	He I	22.1	8.2	11.6	2.3
52.2213	He I	21.6	7.9	11.6	2.0

* Interpolated from data of reference 27.

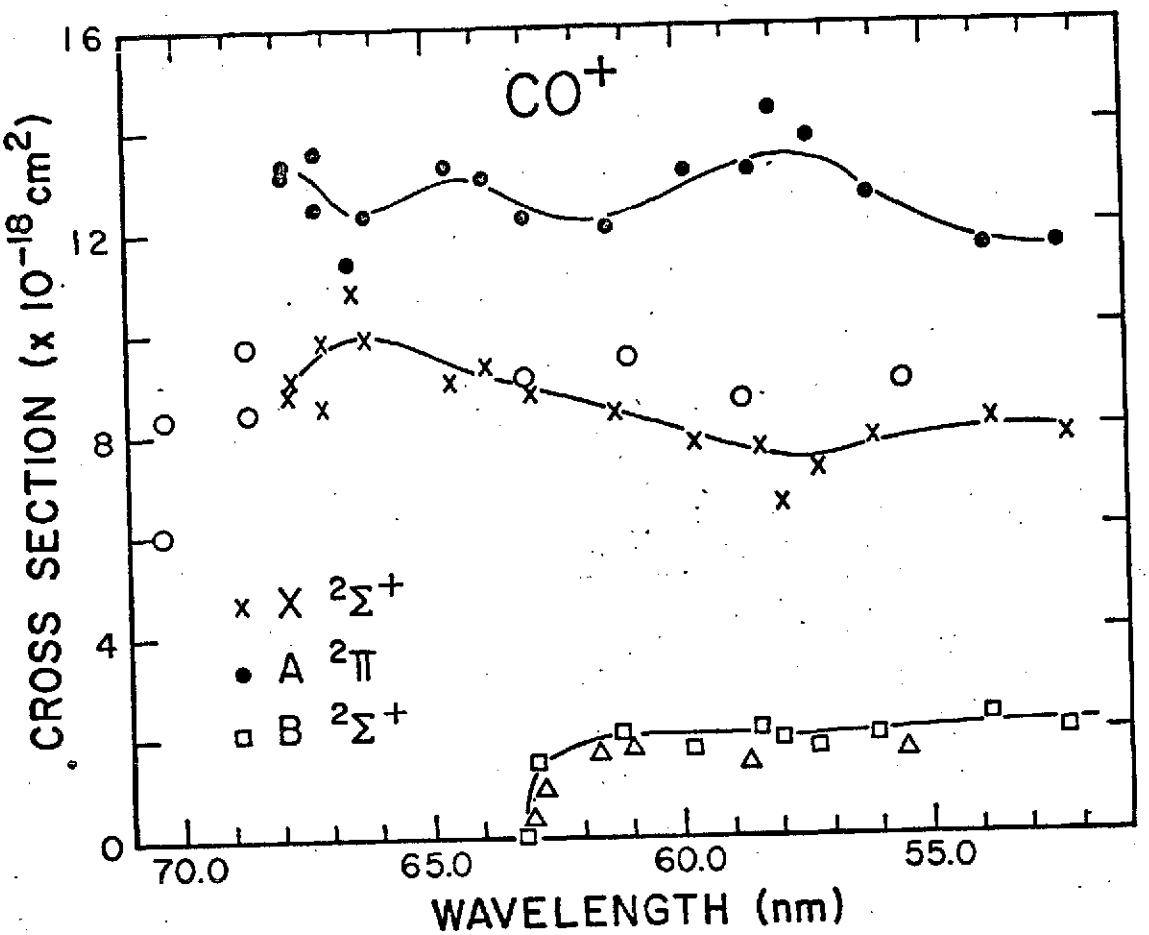

Figure 20. Partial photoionization cross sections for producing the CO^+ states listed. The data points o and Δ are the A-X and B-X fluorescence cross sections respectively from ref. 28.

Table 8. Vibrational Intensity Distributions and Franck-Condon Factors for Continuum Photo-ionization of CO ($X\ ^1\Sigma^+$)

CO^+ State	v	Experimental Intensity	FCF[19]
$X\ ^2\Sigma^+$	0	100.0	100.0
	1	3.46 ± 0.27	3.84
$A\ ^2\Pi$	0	39.4 ± 2.4	37.3
	1	83.4 ± 1.4	82.1
	2	100.0 ± 3.1	100.0
	3	86.7 ± 1.6	89.5
	4	67.8 ± 1.9	66.0
	5	50.3 ± 1.7	42.6
	6	24.2 ± 1.3	25.0
	7	14.8 ± 0.5	13.7
	8	8.31 ± 0.47	7.15
	9	5.08 ± 0.97	3.59
	10	2.53 ± 0.56	1.75
	11	1.03 ± 0.22	0.84
$B\ ^2\Sigma$	0	100.0	100.0
	1	35.0 ± 1.0	35.4
	2	7.75 ± 1.61	7.06

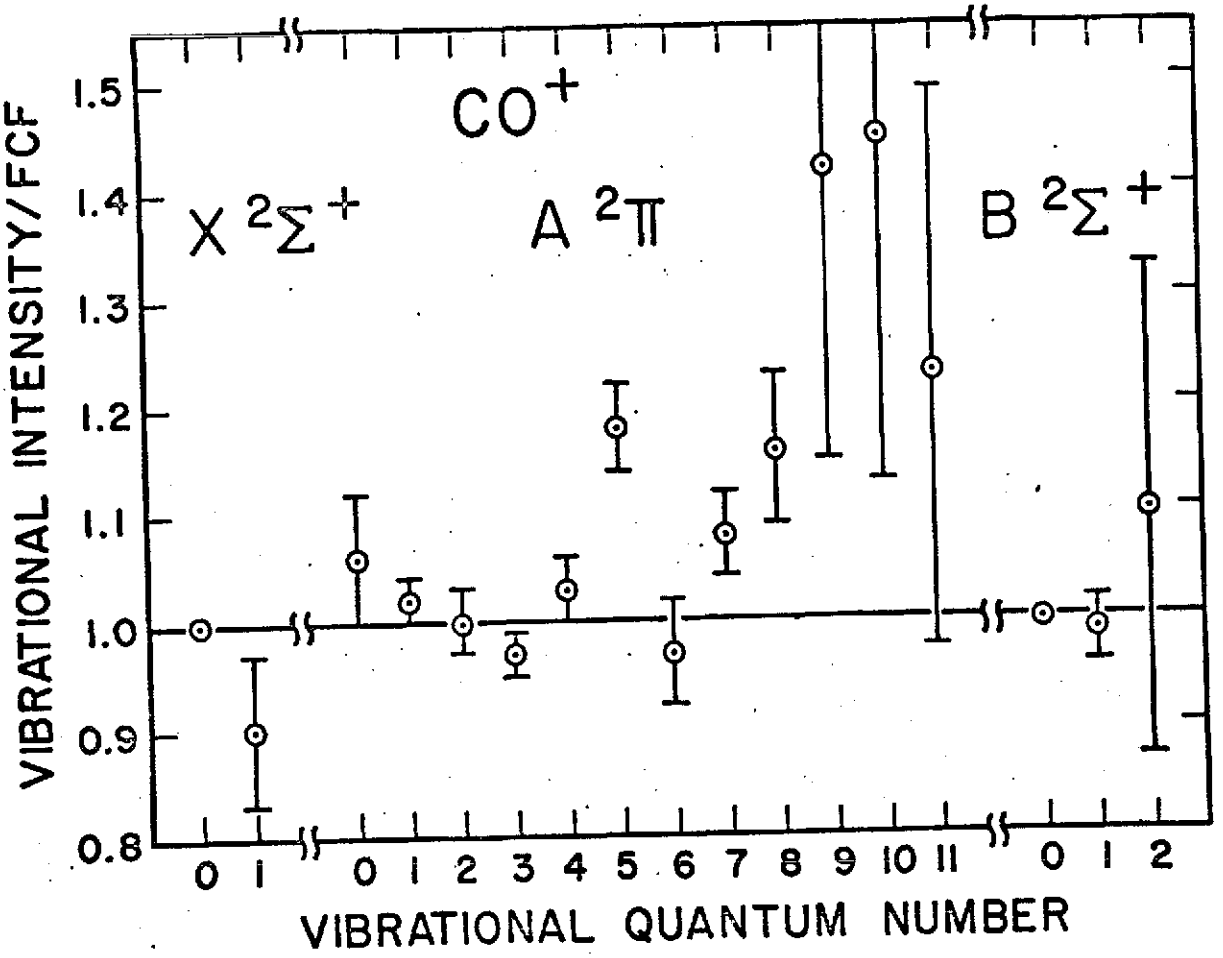

Figure 21. Vibrational intensity distributions for continuum photoionization of carbon monoxide.

Carbon Dioxide

(1) Branching Ratios

Photoelectron spectra were recorded from carbon dioxide at wavelengths ranging from 70.5 to 51.9 nm. A spectrum recorded at 58.4 nm (He I) with a pass energy is shown in Figure 22. At the corresponding resolution of 45 meV, the CO_2^+ A $^2\Pi_u$ v=5 and v=6 peaks are not resolved from the wings of the B $^2\Sigma_u^+$ v=0 peak. A spectrum taken at 58.4 nm with a pass energy of 0.75 eV, over the A $^2\Pi_u$ and B $^2\Sigma_u^+$ vibrational structure, is plotted in Figure 23. The v=5 and v=6 levels of the A $^2\Pi_u$ state are clearly resolved. The spin-orbit splitting of 11 meV in the A $^2\Pi_u$ peaks[29] is not resolved, largely due to the Doppler broadening of these peaks at a wavelength of 58.4 nm. From this spectrum, we estimate that the A $^2\Pi_u$ v=5 and v=6 levels occupy 9.5% of the v=0 to v=4 intensity. In recording the branching ratios, 9.5% of the v=0 to v=4 intensity was added to the v=0 to v=4 sum to give the integrated A $^2\Pi_u$ intensity and this amount added was subtracted from the intensity measured in the (A $^2\Pi_u$ v=5,6 : B $^2\Sigma_u^+$ v=0) peak to determine the B $^2\Sigma_u^+$ v=0 intensity.

The branching ratios at the various wavelengths are listed in Table 9 and plotted in Figure 24. The extended vibrational structure that characterizes autoionization was not as prevalent in the CO_2 spectra as in N_2 and CO. In fact, extended vibrational structure in the ground state of CO_2^+ was only significant in a spectrum recorded at 77.5965 nm (NII); at this wavelength, only the CO_2^+ ground state is energetically accessible, and the spectrum is not included in Table 9.

The strongest effect of autoionization appeared in the spectrum recorded at a wavelength of 66.1869 nm (Ar II). This wavelength coincides with a "window resonance" in the CO_2 photoabsorption cross section.[30] The vibrational distributions in each of the X $^2\Pi_g$, A $^2\Pi_u$, and B $^2\Sigma_u^+$ bands

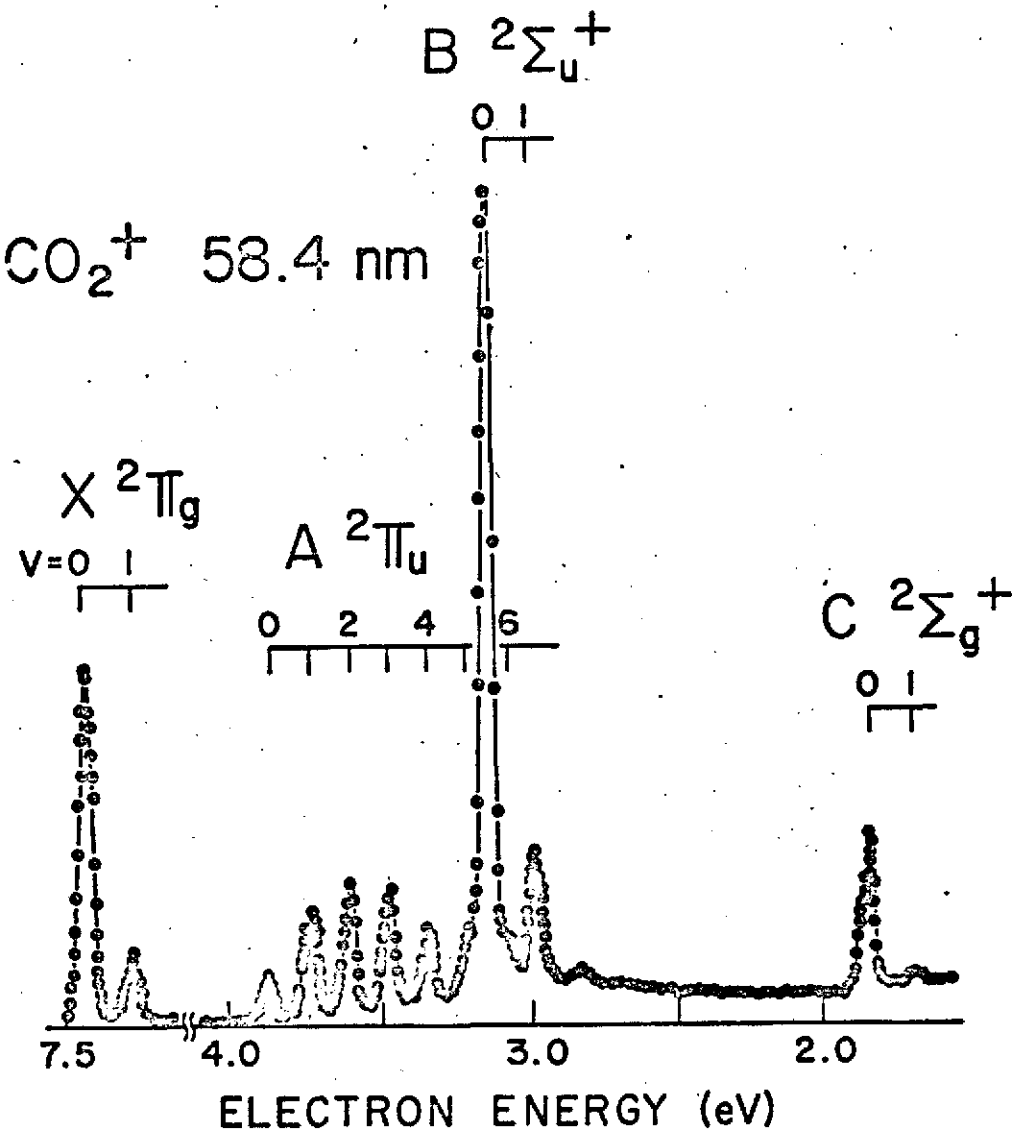

Figure 22. Photoelectron spectrum recorded from carbon dioxide at a wavelength of 58.4 nm.

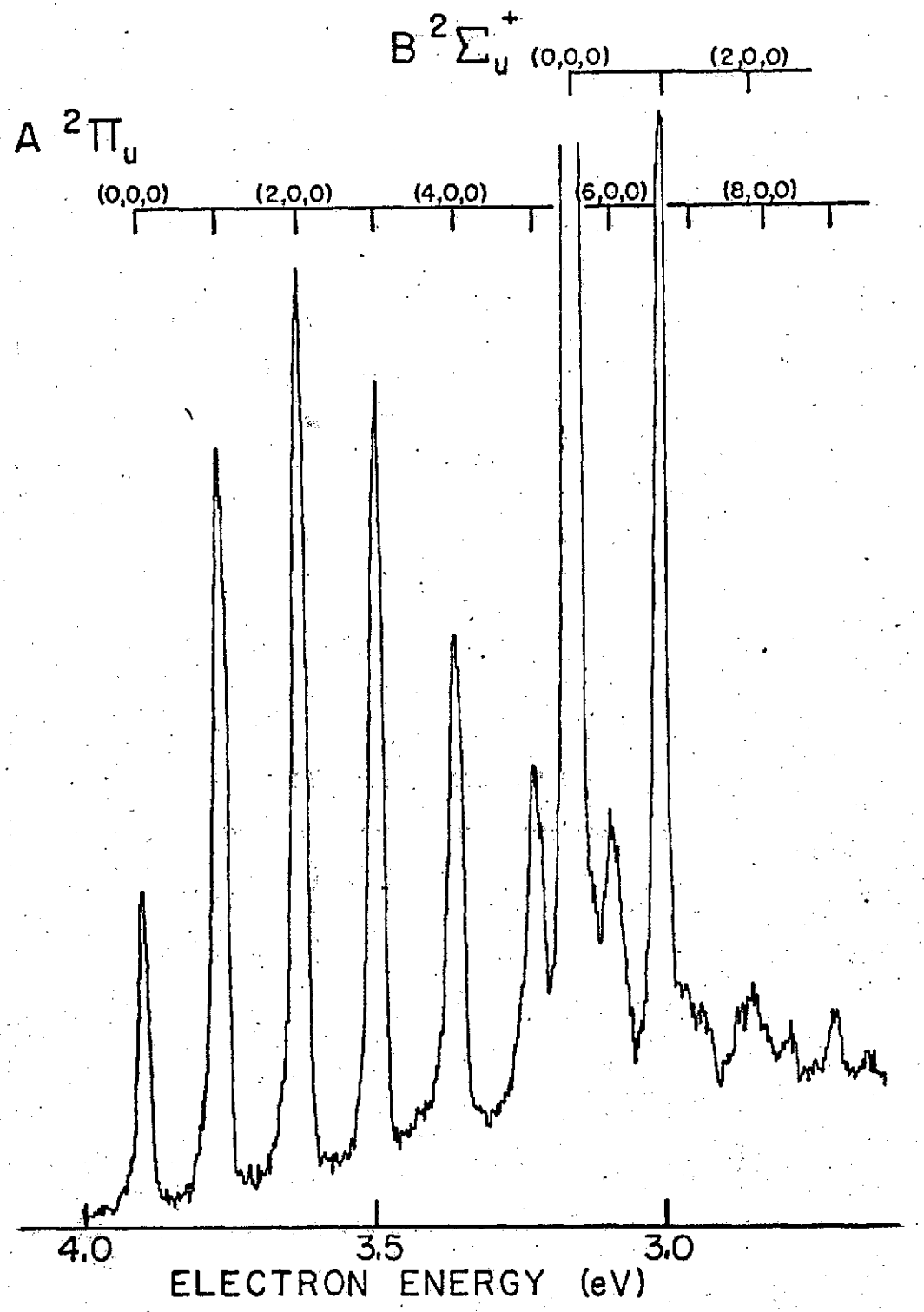

Figure 23. High resolution recording of the portion of the carbon dioxide photoelectron spectrum at 58.4 nm covered by the CO_2^+ A $^2\Pi_u$ and B $^2\Sigma_u^+$ electronic states.

Table 9. Photoelectron Branching Ratios for Photoionization of CO_2 ($X\ ^1\Sigma^+$) to the CO_2^+ ($X\ ^2\Pi_g$), ($A\ ^2\Pi_u$), ($B\ ^2\Sigma_u$), and ($C\ ^2\Sigma_g$) States.

Wavelength (nm)	Origin	Branching Ratio (%)			
		$X\ ^2\Pi_g$	$A\ ^2\Pi_u$	$B\ ^2\Sigma_u$	$C\ ^2\Sigma_g$
70.4523	Ar II	74.6	25.4		
69.80	Ar II	65.4	34.6		
67.7952	Ar II	42.6	32.4	25.0	
67.1852	Ar II	36.0	26.8	37.2	
67.15	N II	36.8	25.5	37.7	
66.4563	Ar II	35.1	25.2	39.7	
66.1869	Ar II	41.1	30.0	28.9	
64.50	N II	34.2	23.8	42.0	
63.7282	Ar III	38.5	26.3	30.9	4.3
61.2372	Ar II	39.7	26.2	30.4	3.7
59.7700	Ar II	35.8	25.2	35.8	3.2
58.4334	He I	33.7	25.6	37.0	3.7
58.0263	Ar II	33.0	26.9	36.6	3.4
57.27	Ar II	32.1	27.7	36.4	3.7
56.0223	Ar II	32.6	26.5	35.1	5.7
55.5766	Ar II	29.6	28.0	37.8	4.6
54.0806	Ar II	29.9	29.2	35.8	5.1
53.7030	He I	30.0	28.6	36.4	5.1
52.2213	He I	30.3	27.1	36.8	5.7
51.91	Ar II	31.2	29.4	33.6	5.8

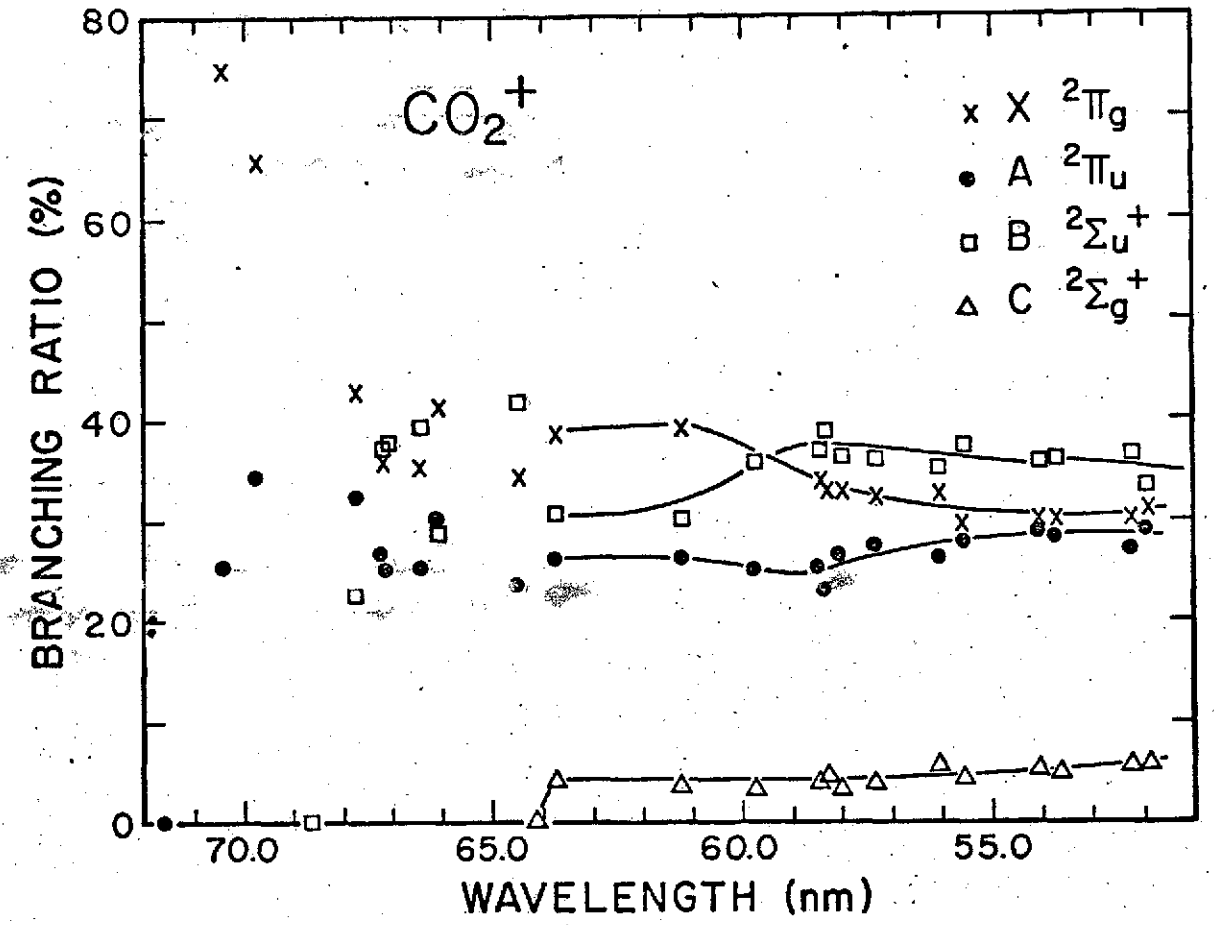

Figure 24. Branching ratios for photoionization of carbon dioxide to the ionic states listed.

remained the same as the continuum distributions at 58.4 nm, but the A $^2\Pi_u$ to B $^2\Sigma_u^+$ intensity ratio changed from 0.66 at surrounding wavelengths to 1.04 at the resonance.

At wavelengths below 63.7 nm, the literature values of the photoionization cross section were interpolated to the wavelengths of the present study and multiplied by the branching ratios to determine partial photoionization cross sections for ionization to each of the X $^2\Pi_g$, A $^2\Pi_u$, B $^2\Sigma_u^+$, and C $^2\Sigma_g^+$ states of CO_2^+. These are listed in Table 10 and plotted in Figure 25. Also plotted in Figure 25 are the cross sections for producing the CO_2^+ A $^2\Pi_u$ to X $^2\Pi_g$ and B $^2\Sigma_u^+$ to X $^2\Pi_g$ fluorescent bands as a function of the exciting wavelength.[31] While the sum of the A $^2\Pi_u$ and B $^2\Sigma^+$ cross sections for the fluorescence and photoelectron experiments are in reasonable agreement, the cross section for the A $^2\Pi_u$ fluorescence emission system is higher than that for initial production of the A $^2\Pi_u$ level (which is measured in the photoelectron experiment), while the B $^2\Sigma_u^+$ fluorescence emission system has a lower cross section than that for the production of the B $^2\Sigma_u^+$ level. This suggests that some of the initial population of the B $^2\Sigma_u^+$ level is transferred to the A $^2\Pi_u$ level. The mechanism of this transfer is unknown, although possible explanations have been discussed in the literature.[32]

(2) Continuum Vibrational Intensity Distributions

Several photoelectron spectra were recorded at 58.4 nm to determine the vibrational intensity distribution for photoionizing transitions from CO_2 X $^1\Sigma^+$ to each of the X $^2\Pi_g$, A $^2\Pi_u$, B $^2\Sigma_u^+$, and C $^2\Sigma_g$ electronic states of CO_2^+. The results are listed in Table 11.

Table 10. Partial Cross-Sections for Photoionization of CO_2 ($X\ ^1\Sigma^+$) to the CO_2^+ ($X\ ^2\Pi_g$), ($A\ ^2\Pi_u$), ($B\ ^2\Sigma_u$), and ($C\ ^2\Sigma_g$) States.

Wavelength (nm)	Origin	Cross-section (x 10^{-18} cm^2)				
		Total*	$X\ ^2\Pi_g$	$A\ ^2\Pi_u$	$B\ ^2\Sigma_u$	$C\ ^2\Sigma_g$
63.7282	Ar III	34.5	13.3	9.1	10.7	1.5
61.2372	Ar II	35.7	14.2	9.4	10.9	1.3
59.7700	Ar II	37.0	13.2	9.3	13.2	1.9
58.4334	He I	37.5	12.6	9.6	13.9	1.4
58.0263	Ar II	37.5	12.4	10.1	13.7	1.3
57.27	Ar II	37.2	11.9	10.3	13.5	1.4
56.0223	Ar II	36.4	11.9	9.6	12.8	2.1
55.5766	Ar II	35.7	10.6	10.0	13.5	1.6
54.0806	Ar II	34.3	10.3	10.0	12.3	1.7
53.7030	He I	34.2	10.3	9.8	12.4	1.7
52.2213	He I	32.2	9.8	8.7	11.8	1.8
51.91	Ar II	32.0	10.0	9.4	10.8	1.9

* Interpolated from the data of reference 27.

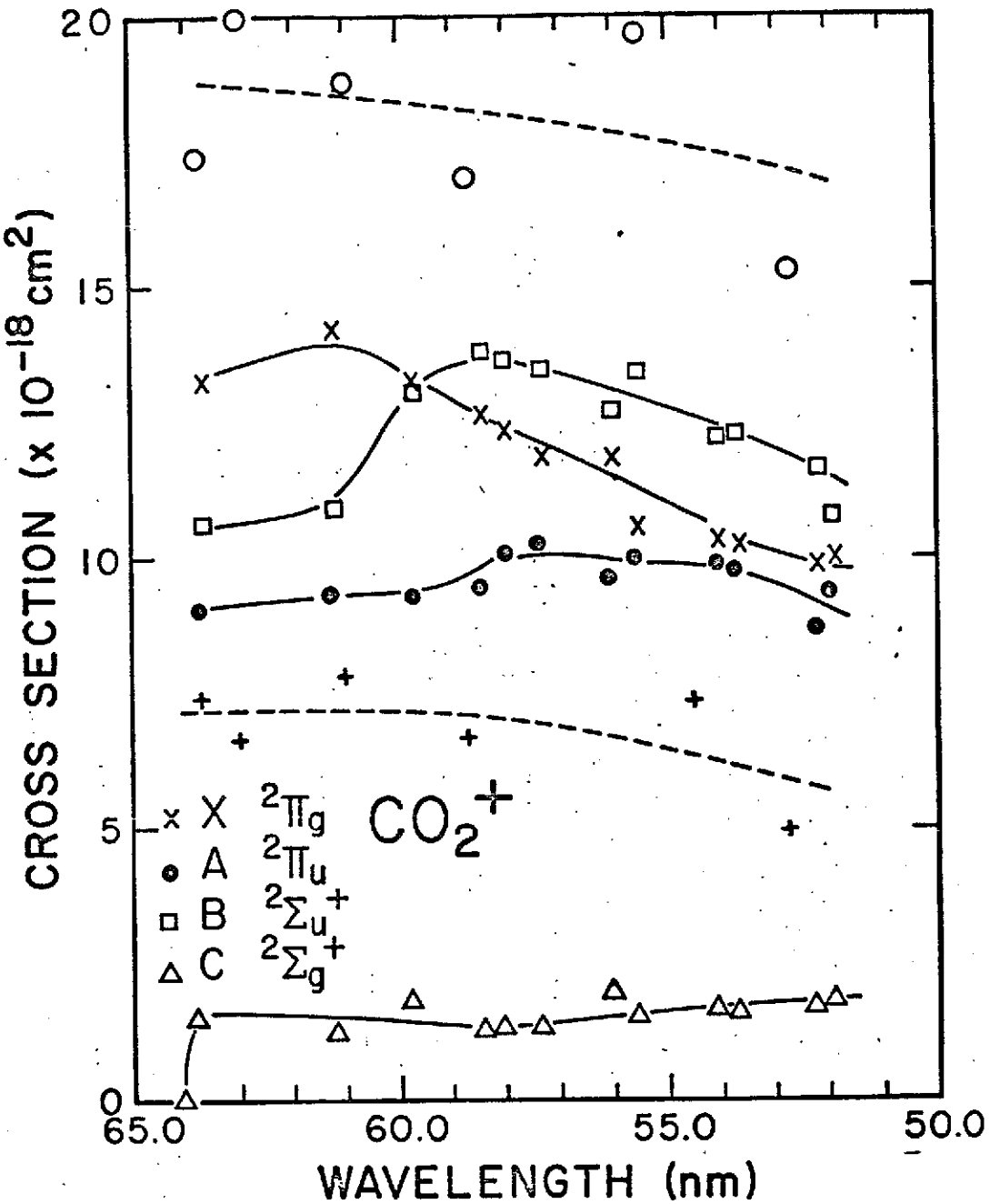

Figure 25. Partial photoionization cross sections for producing the CO_2^+ states listed. The data points o and + represent the A-X and B-X fluorescence cross sections respectively (data from ref. 31).

Table 11. Vibrational Intensity Distributions for Continuum Photoionization of CO_2 ($X\ ^1\Sigma^+$).

CO_2^+ State	(v,o,o)	Experimental Intensity
$X\ ^2\Pi_g$	0	100
	1	18.4
	2	
$A\ ^2\Pi_u$	0	32.6
	1	85.5
	2	100
	3	74.8
	4	54.7
	5	24.7
	6	11.8
$B\ ^2\Sigma_u^+$	0	100
	1	15.7
	2	2.3
$C\ ^2\Sigma_g^+$	0	100
	1	6.5
	2	

IV. CONCLUSIONS

The goal of the present work was to obtain partial photoionization cross sections of N_2, CO, and CO_2. This has been achieved over the wavelength range 53 to 75 nm. Between 53 and 65 nm the partial cross sections do not exhibit discrete structure. Thus, these results can be used directly in conjunction with solar radiation wavelengths in this region for calculating the ionizing effects on an atmosphere containing these gases.

REFERENCES

1. J. A. R. Samson, Techniques of Vacuum Ultraviolet Spectroscopy, Wiley, N.Y. (1967), p. 150.
2. H. Hinteregger and L. Hall, Solar Phys. 6, 175 (1969).
3. J. L. Gardner and J. A. R. Samson, J. Electron Spectrosc. 2, 267 (1973).
4. J. A. R. Samson and J. L. Gardner, J. Opt. Soc. Am. 62, 856 (1972).
5. L. J. Kieffer, Atomic Data 2, 293 (1971).
6. J. A. R. Samson, Advan. Atom. Mol. Phys. 2, 177 (1966).
7. J. A. R. Samson and R. B. Cairns, Phys. Rev. 173, 80 (1968).
8. G. Herzberg, Spectra of Diatomic Molecules, Van Nostrand, New Jersey, (1950), p. 561.
9. R. T. Poole, R. C. G. Leckey, J. Liesegang and J. G. Jenkin, J. Phys. E. (Sci. Instr.) 6, 226 (1973).
10. P. C. Kemeny, A. D. McLachlan, F. L. Battye, R. T. Poole, R. C. G. Leckey, J. Liesegang and J. G. Jenkin, Rev. Sci. Instr. 44, 1197 (1973).
11. R. L. Arnoldy, P. O. Isaacson, D. F. Gats and L. W. Choy, Rev. Sci. Instr. 44, 172 (1973).
12. R. L. Kelly, NRL Report 6648 (1968).
13. M. Ogawa and Y. Tanaka, Can. J. Phys. 40, 1593 (1962).
14. A. J. Blake and J. H. Carver, J. Chem. Phys. 47, 1038 (1967).
15. R. E. Huffman, Y. Tanaka and J. C. Larrabee, J. Chem Phys. 39, 910 (1963).
16. J. A. R. Samson and R. B. Cairns, J. Geophys. Res. 69, 4583 (1964); J. Opt. Soc. Am. 55, 1035 (1965).
17. D. L. Judge and G. L. Weissler, J. Chem. Phys. 48, 4590 (1968).

18. H. C. Tuckwell, J. Phys. B. 3, 293 (1970).

19. D. L. Albritton, A. L. Schmeltekopf and R. N. Zare, Diatomic Intensity Factors (Wiley, N.Y., in preparation).

20. D. G. Streets, A. W. Potts and W. C. Price, Int. J. Mass Spectrom. Ion Phys. 10, 123 (1972).

21. Y. Itikawa, J. Electron Spectrosc. 2, 125 (1973).

22. T. A. Carlson, Chem. Phys. Letters 9, 23 (1971).

23. M. J. Van der Wiel and C. E. Brion, J. Electron Spectrosc. 1, 309 (1972/73).

24. T. A. Carlson and A. E. Jonas, J. Chem. Phys. 55, 4913 (1971).

25. J. L. Bahr, A. J. Blake, J. H. Carver, J. L. Gardner and Vijay Kumar, J. Quant. Spectrosc. Radiat. Transfer 12, 59 (1972).

26. R. E. Huffman, J. C. Larrabee and Y. Tanaka, J. Chem. Phys. 40, 2261 (1964).

27. R. B. Cairns and J. A. R. Samson, J. Geophys. Res. 70, 99 (1965); J. Opt. Soc. Am. 56, 526 (1966).

28. D. L. Judge and L. C. Lee, J. Chem. Phys. 57, 455 (1972).

29. Y. Tanaka and M. Ogawa, Can. J. Phys. 40, 879 (1962).

30. Y. Tanaka, A. S. Jursa and F. J. LeBlanc, J. Chem. Phys. 32, 1199 (1960).

31. L. C. Lee and D. L. Judge, J. Chem. Phys. 57, 4443 (1972).

32. J. A. R. Samson and J. L. Gardner, J. Geophys. Res. 78, 3663 (1973).